Redox Biology 73 (2024) 103184

Contents lists available at ScienceDirect

Redox Biology

journal homepage: www.elsevier.com/locate/redox

Sirt5 improves cardiomyocytes fatty acid metabolism and ameliorates cardiac lipotoxicity in diabetic cardiomyopathy *via* CPT2 de-succinylation

Maoxiong Wu [a,b,c,1], Jing Tan [d,1], Zhengyu Cao [a,b,c,1], Yangwei Cai [a,b,c,1], Zhaoqi Huang [a,b,c], Zhiteng Chen [a,b,c], Wanbing He [a,b,c], Xiao Liu [a,b,c], Yuan Jiang [a,b,c], Qingyuan Gao [a,b,c], Bingqing Deng [a,b,c], Jingfeng Wang [a,b,c,**], Woliang Yuan [a,b,c,***], Haifeng Zhang [a,b,c,*], Yangxin Chen [a,b,c,****]

[a] *Department of Cardiology, Sun Yat-sen Memorial Hospital of Sun Yat-sen University, Guangzhou, 510120, China*
[b] *Guangzhou Key Laboratory of Molecular Mechanisms of Major Cardiovascular Disease, Sun Yat-sen Memorial Hospital of Sun Yat-sen University, Guangzhou, 510120, China*
[c] *Guangdong Provincial Key Laboratory of Arrhythmia and Electrophysiology, Sun Yat-sen Memorial Hospital of Sun Yat-sen University, Guangzhou, 510120, China*
[d] *Laboratory Animal Center and Department of Biochemistry, Institute of Guangdong Engineering and Technology Research Center for Disease-Model Animals, Zhongshan School of Medicine, Sun Yat-sen University, Guangzhou, 510080, China*

A R T I C L E I N F O

Keywords:
Sirtuin 5
Diabetic cardiomyopathy
Carnitine palmitoyltransferase 2
Lysine succinylation
Fatty acid oxidation

A B S T R A C T

Rationale: The disruption of the balance between fatty acid (FA) uptake and oxidation (FAO) leads to cardiac lipotoxicity, serving as the driving force behind diabetic cardiomyopathy (DbCM). Sirtuin 5 (*Sirt5*), a lysine de-succinylase, could impact diverse metabolic pathways, including FA metabolism. Nevertheless, the precise roles of *Sirt5* in cardiac lipotoxicity and DbCM remain unknown.

Objective: This study aims to elucidate the role and underlying mechanism of *Sirt5* in the context of cardiac lipotoxicity and DbCM.

Methods and results: The expression of myocardial *Sirt5* was found to be modestly elevated in diabetic heart failure patients and mice. Cardiac dysfunction, hypertrophy and lipotoxicity were exacerbated by ablation of *Sirt5* but improved by forced expression of *Sirt5* in diabetic mice. Notably, *Sirt5* deficiency impaired FAO without affecting the capacity of FA uptake in the diabetic heart, leading to accumulation of FA intermediate metabolites, which mainly included medium- and long-chain fatty acyl-carnitines. Mechanistically, succinylomics analyses identified carnitine palmitoyltransferase 2 (CPT2), a crucial enzyme involved in the reconversion of fatty acyl-carnitines to fatty acyl-CoA and facilitating FAO, as the functional succinylated substrate mediator of *Sirt5*. Succinylation of Lys424 in CPT2 was significantly increased by *Sirt5* deficiency, leading to the inactivation of its enzymatic activity and the subsequent accumulation of fatty acyl-carnitines. CPT2 K424R mutation, which mitigated succinylation modification, counteracted the reduction of enzymatic activity in CPT2 mediated by *Sirt5* deficiency, thereby attenuating *Sirt5* knockout-induced FAO impairment and lipid deposition.

Conclusions: Sirt5 deficiency impairs FAO, leading to cardiac lipotoxicity in the diabetic heart through the succinylation of Lys424 in CPT2. This underscores the potential roles of *Sirt5* and CPT2 as therapeutic targets for addressing DbCM.

* Corresponding authors. Department of Cardiology, Sun Yat-sen Memorial Hospital of Sun Yat-sen University, Guangzhou, 510120, China.
** Corresponding author. Department of Cardiology, Sun Yat-sen Memorial Hospital of Sun Yat-sen University, Guangzhou, 510120, China.
*** Corresponding authors. Department of Cardiology, Sun Yat-sen Memorial Hospital of Sun Yat-sen University, Guangzhou, 510120, China.
**** Corresponding author. Department of Cardiology, Sun Yat-sen Memorial Hospital of Sun Yat-sen University, Guangzhou, 510120, China.
E-mail addresses: wjingf@mail.sysu.edu.cn (J. Wang), yuanwl@mail.sysu.edu.cn (W. Yuan), zhanghf9@mail.sysu.edu.cn (H. Zhang), chenyx39@mail.sysu.edu.cn (Y. Chen).
[1] These authors contributed equally to this study.

https://doi.org/10.1016/j.redox.2024.103184
Received 18 March 2024; Received in revised form 24 April 2024; Accepted 4 May 2024
Available online 5 May 2024

1. Introduction

Diabetic cardiomyopathy (DbCM), which is widely recognized as an important independent cause for heart failure (HF), represents a significant and potentially fatal complication of diabetes-associated cardiac injury [1–3]. In the early stages of DbCM, diastolic dysfunction is the main manifestation, which may progress to systolic dysfunction over time [4]. Even after adjusting for multiple risk factors (e.g., age, hypertension, and coronary artery disease), the incidence of heart failure remains much higher in DbCM patients. Therefore, DbCM is expanded to underscore the heightened susceptibility of the myocardium to dysfunction in diabetic patients [5]. However, clinical trials have revealed that while intensive glucose control may reduce the incidence of myocardial infarction in diabetic patients, it does not decrease the rate of rehospitalization or mortality due to HF [6,7]. Therefore, there is an urgent need to elucidate the underlying mechanisms in order to identify potential therapeutic targets for DbCM.

DbCM is recognized as a cardiac metabolic disorder, characterized by the accumulation of toxic lipid metabolites in the diabetic heart, a phenomenon known as cardiac lipotoxicity [8,9], which could be attributable to the increased fatty acid (FA) uptake by cardiomyocytes and/or the decreased allosteric control of mitochondrial FA uptake and subsequent fully fatty acid oxidation (FAO) [10]. In fact, under DbCM, FAO in cardiomyocytes becomes insufficient to fully metabolize all the ingested FA over time [11–13]. Consequently, excessive FA and FA-derived intermediate metabolites, such as ceramides and diacylglycerol, accumulate in cardiomyocytes, resulting in structural and functional abnormality of the heart and leading to HF [14]. Increased cardiac FAO has long been considered to reduce cardiac glucose utilization and energy expenditure [15]. However, the inhibition of FAO showed sharply conflictive results, ranging from beneficial to unchanged to harmful effects [16–19]. One of the most plausible explanation of these contradictory results could be the different targets and strategies for FAO inhibition or different animal models used. Therefore, it is necessary to explore more targets that are effective in the regulation of FAO and DbCM.

Sirtuins, evolutionarily conserved lysine deacylases that rely on nicotinamide adenine dinucleotide, play a pivotal role in the pathogenesis of cardiometabolic diseases [20]. The sirtuin family comprises seven members, including *Sirt*1-7, of which *Sirt1* [21], *Sirt2* [22], *Sirt3* [23], and *Sirt6* [23] have been demonstrated to be crucial in DbCM. While *Sirt4* [24], *Sirt5* [25], and *Sirt7* [26] have been implicated in the regulation of fatty acid metabolism, their specific roles in DbCM remain unclear. Unlike other sirtuins, *Sirt5* mediates lysine de-succinylation, de-malonylation, and de-glutarylation in addition to de-acetylation. *Sirt5* is prominently expressed in the heart, and its absence disrupts FAO and diminishes physiological cardiac function through the succinylation of the mitochondrial trifunctional enzyme subunit alpha [25]. Global knockout of *Sirt5* has been shown to increase mortality in mice subjected to cardiac stress overload induced by transverse aortic constriction [27]. These findings suggest that *Sirt5* regulates cardiac metabolism and function. However, the precise roles of *Sirt5* in the pathogenesis of DbCM remains unclear.

In this study, we present convincing evidence supporting the involvement of *Sirt5* in cardiac lipotoxicity and DbCM. Our findings revealed a modest increase in myocardial *Sirt5* expression in diabetic HF patients and db/db mice. Gain- and loss-of-function experiments identified *Sirt5* as an important inhibitor of cardiac dysfunction and hypertrophy in diabetic mice. Ablation of *Sirt5* contributed to cardiac FAO dysfunction, exacerbating cardiac lipotoxicity and dysfunction. Mechanistically, we demonstrated that *Sirt5* deficiency mediated Lys424 succinyaltion of CPT2 to inactivate its enzyme activity, which led to the cardiac FAO impairment and lipids deposition in cardiomyocytes. Our study unveiled a novel role of *Sirt5* and its mediated succinylation of CPT2 in modulating FAO, potentially elucidating the mechanism by which *Sirt5* deficiency exacerbates cardiac lipotoxicity and DbCM. These findings suggest that *Sirt5* and CPT2 could represent promising therapeutic targets in the context of DbCM.

2. Materials and methods

2.1. DbCM models

The global *Sirt5* knockout mouse model (C57BL/6-*Sirt5*^{tm1cyagen}) was created by CRISPR/Cas-mediated genome engineering. Briefly, *Sirt5* gene (NCBI Reference Sequence: NM_178848; Ensembl: ENSMUSG00000054021) is located on mouse chromosome 13. Nine exons are identified, with the ATG start codon in exon 2 and the TAA stop codon in exon 9 (Transcript Sirt5-211: ENSMUST00000223194). Exon 3 was selected as the target site, this region contains 134 bp coding sequence. gRNA1 (matching the forward strand): GCTGAGCCGTCTTTTACTATTGG. gRNA2 (matching the reverse strand): ATTTGCTCCCGTAGTCATCGGGG. Ribonucleoprotein (RNP) was co-injected with the gRNAs into fertilized eggs for KO mouse production. The pups were genotyped by PCR followed by sequencing analysis. The PCR Primers for genotyping: Forward primer: 5′-TGGTGACAATGCCTTTCCTCTGAG-3′, Reverse primer: 5′-GGAGCCAGAGACTACTGAGCATC-3’. Homozygotes: ~550 bp. Heterozygotes: ~550 bp/325 bp/973 bp. Wildtype allele: 325 bp/973 bp (Note: If DNA sample is not very pure or enough PCR extension time, the 973 bp PCR product may not be amplified). The heterozygous *Sirt5* knockout mice (*Sirt5*$^{+/-}$) were obtained from Cyagen Biosciences, and were crossed to generate littermates with the following genotypes: *Sirt5*$^{-/-}$ (the SIRT5 KO mice), *Sirt5*$^{+/-}$ (the heterozygous mice) and *Sirt5*$^{+/+}$ (the wild-type control mice). C57BL/6-*Sirt5*^{tm1cyagen} was the strain name of the mice, and all of these mice were on the C57BL/6 N background. Male C57BLKsJ-db/db mice were obtained from GemPharmatech, with age-matched male C57BLKsJ-m/m mice serving as controls. The mice were group-housed in a 12-h light/dark cycle environment with ad libitum access to rodent chow and tap water. All animal procedures adhered to the Guide for the Care and Use of Laboratory Animals published by the US National Institutes of Health and were approved by the Institutional Animal Care and Use Committee (IACUC) of Sun Yat-sen University [28]. Euthanasia for terminal organ harvest was conducted by the IACUC approved method. In summary, euthanasia was conducted through inhalant anesthetic overdose followed by exsanguination. A precision vaporizer with an induction chamber and waste gas scavenger was utilized to administer >4.5 % Isoflurane in oxygen, which was continued until respiratory arrest persisted for >60 s. Subsequently, the chamber was flushed with oxygen only, the animals were removed, and rapid exsanguination was carried out *via* vena cava puncture to ensure euthanasia, followed by prompt organ harvest.

8-week-old WT and *Sirt5*$^{-/-}$ male mice were randomly divided into HFD/STZ group and control group. Mice in the HFD/STZ group received intraperitoneal injections of low-dose STZ (30 mg/kg, dissolved in citric acid buffer) after a 12-h fast, administered daily for 5 consecutive days, and were simultaneously placed on a HFD for a duration of 24 weeks. Mice in the control group were injected with an equivalent volume of citric acid buffer and were fed a standard chow diet. The HFD consisted of 20 kcal% carbohydrate, 20 kcal% protein, and 60 kcal% fat, while the chow diet comprised 70 kcal% carbohydrate, 20 kcal% protein, and 10 kcal% fat. Both the high-fat diet (D12492) and chow diet (D12450B) were procured from the Research Diets, Inc. Body weight and fasting blood glucose levels of the mice were monitored every 6 weeks. Following the 24-week induction period, cardiac function and left ventricular pressure were assessed using echocardiography and left ventricular catheterization, respectively. Glucose tolerance test (GTT), insulin tolerance test (ITT), and FA uptake were conducted prior to sacrifice. Blood samples were collected for the quantification of cholesterol, triglycerides (TG), and insulin. Heart tissues were excised and weighted (Heart weight, HW) before using for proteomics, metabolomics, TG quantification, and pathological staining. Cardiomyocytes

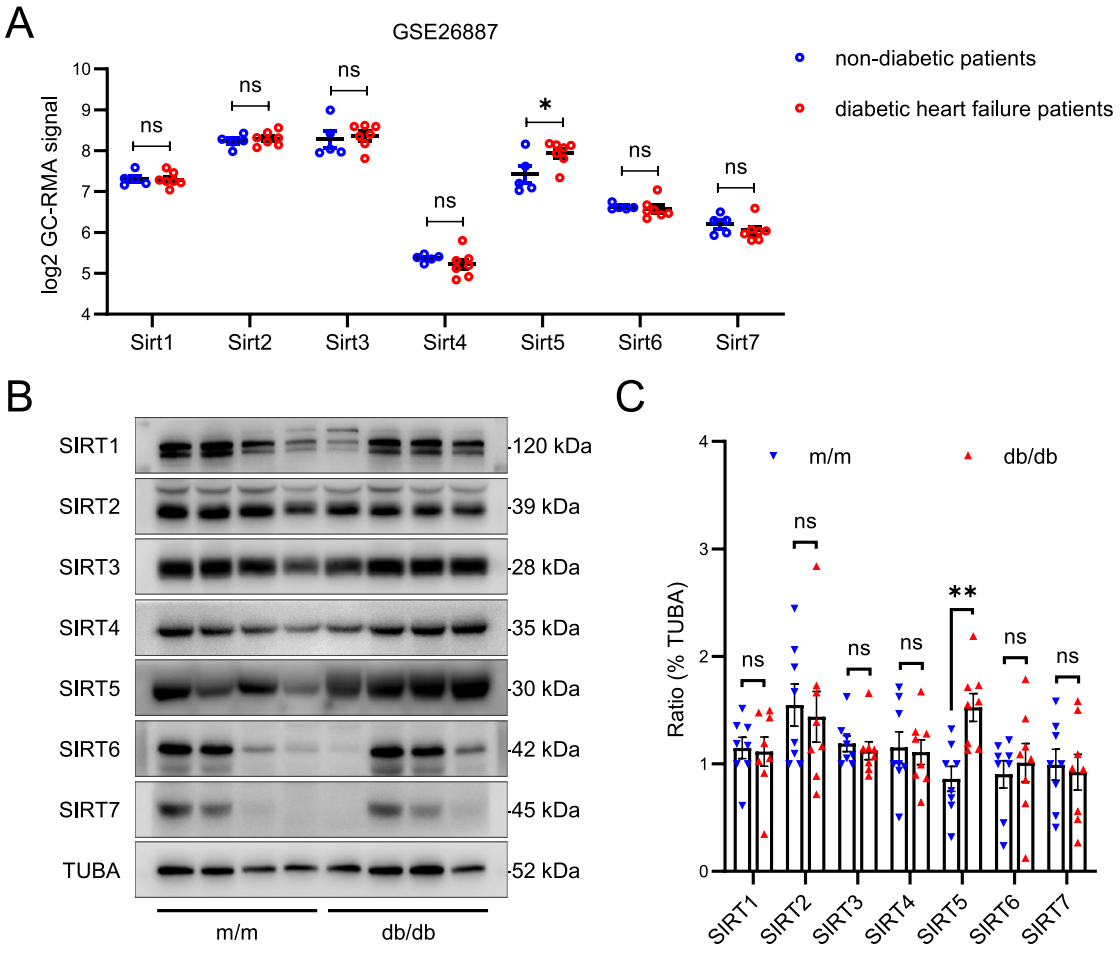

Fig. 1. Myocardial expression of *Sirt5* in diabetic patients and mice. A, Myocardial sirtuins (*Sirt*1-7) expression in non-diabetic (n = 5) and diabetic HF (n = 7) patients in the GSE26887 from GEO dataset. Raw data of log2 GC-RMA signal were analyzed using Student's t-test. **B**, Representative Western blot of myocardial sirtuins (*Sirt*1-7) protein expression in 32-week-old male m/m mice and db/db mice (n = 8/group), TUBA (α-tubulin) was used as the loading control. **C**, Statistical analysis of the Western blot using Student's t-test. Data are expressed as mean ± SEM. ns, no significant, $^{*}P < 0.05$, $^{**}P < 0.01$.

were isolated from the myocardium for FAO detection. Tibial length (TL) was measured.

20-week-old m/m and db/db mice were randomly allocated to receive AAV9-*Sirt5* or AAV9-control *via* tail vein injection. Subsequently, the mice were maintained on a chow diet for a duration of 8 weeks. Baseline and end-of-study assessments included the examination of body weight and fasting blood glucose levels. Echocardiography was conducted to assess the systolic and diastolic function of the mice prior to sacrifice. HW and TL were measured. Blood samples were collected for the quantification of cholesterol, TG, and insulin. Additionally, heart tissues were excised for TG quantification and pathological staining.

2.2. Cardiac sirtuins expression in diabetic HF patients

A diabetic HF-related expression profiling microarray (GSE26887) was obtained from the Gene Expression Omnibus (GEO) repository. The dataset comprised LV cardiac biopsies from five control non-HF patients and seven diabetic HF patients, with gene expression assessed using the Affymetrix GeneChips Human Gene 1.0 ST array. Log2 GC-RMA signals of *Sirt*1-7 from the dataset were used to compare their gene expressions. All procedures were performed according to the Declaration of Helsinki and were approved by the local medical ethics review committees.

2.3. Cardiac functions

Upon completion of the intervention, 1 % continues inhale isoflurane anesthesia was used to anesthetized the mice. Echocardiograms were acquired and analyzed using a Visual Sonics Echo System (Vevo2100, FUJIFILM VisualSonics, Inc, Toronto, Canada) and MicroScan Transducer (MS-400, 30 MHz, FUJIFILM VisualSonics, Inc) according to our previous publication [28]. Left ventricular (LV) end-diastolic dimension, LV end-systolic dimension, LV mass (LVM), E wave, A wave, and e' wave were measured utilizing Vevo LAB software (Version 3.1.1, FUJIFILM Visualsonics, Inc). LV ejection fraction (LVEF), LV fractional shortening (LVFS), E/A ratio, and E/e' ratio were calculated in accordance with previously established methods [29]. Subsequently, a catheter manometer (PowerLab, ADInstruments, Bella Vista, Australia) was employed to monitor LV pressure, inserted *via* the right carotid artery into the left ventricle. Data were recorded, and dp/dt_{max} and dp/dt_{min} were calculated using LabChart (ADInstruments). All the techniques were approved by the institutional IACUC.

2.4. AAV9 construction and transfection

AAV9 was utilized to facilitate the overexpression of *Sirt5* in cardiomyocytes for the *in vivo* study. The AAV expression vector pAAV-CMV-Sirt5-3FLAG-P2A-mNeonGreen-CW3SL was synthesized and

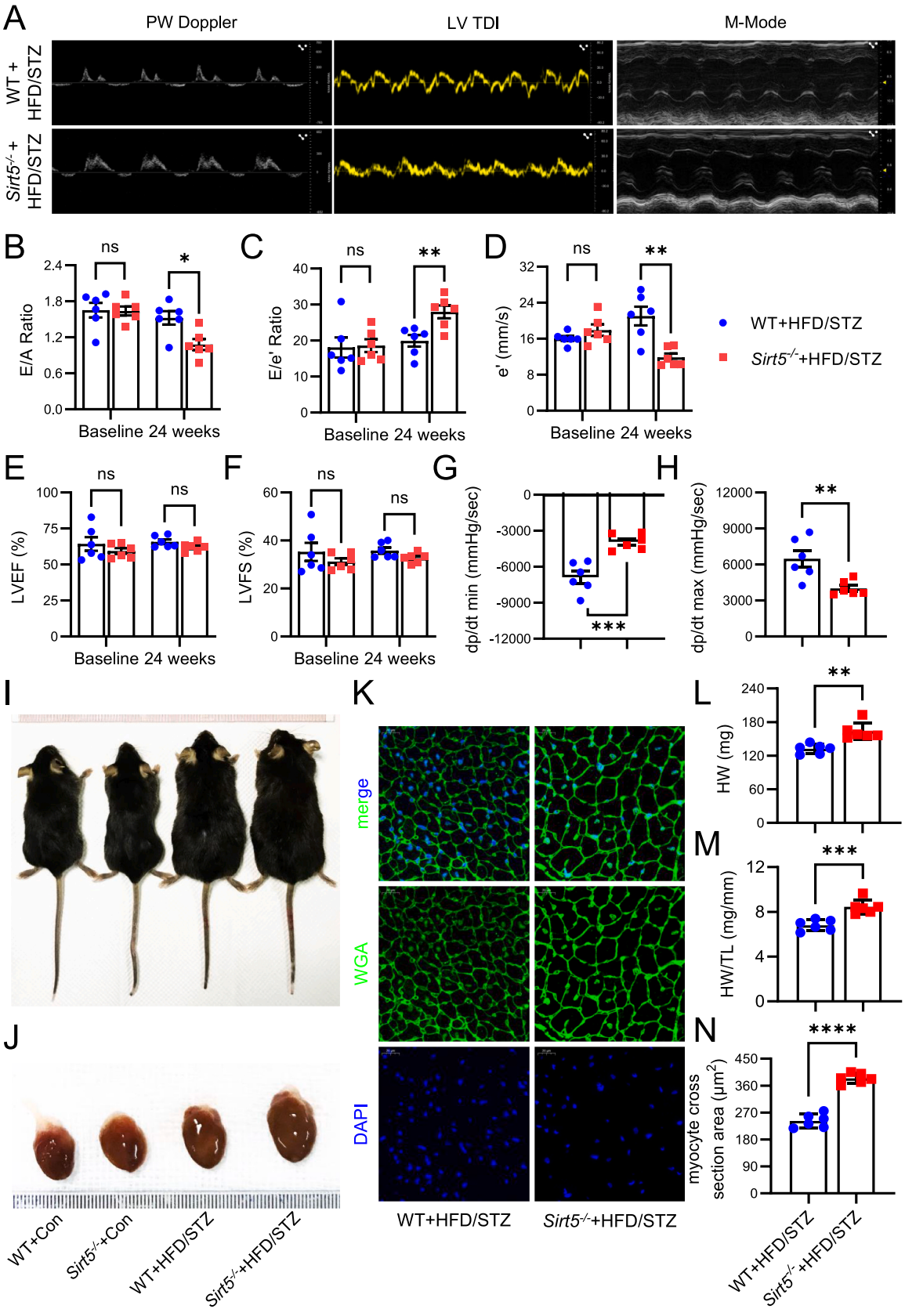

(caption on next page)

Fig. 2. Effects of *Sirt5* knockout on HFD/STZ-induced cardiac dysfunction and hypertrophy. A, Representative echocardiographic images of PW Doppler (*left*), LV TDI (Left ventricular tissue doppler imaging) (*middle*) and M-Mode (*right*) in WT and *Sirt5*$^{-/-}$ mice after HFD/STZ induction (n = 6/group). **B–F**, Statistical analyses of E/A Ratio (**B**), E/e' Ratio (**C**), e' (**D**), LVEF (**E**) and LVFS (**F**) of the above mice. **G-H**, Statistical analyses of LV pressure parameters, including dp/dt_{min} (**G**) and dp/dt_{max} (**H**) of the above mice (n = 6/group). **I-J**, Representative macroscopic images of the mice (**I**) and their hearts (**J**). **K**, Representative immunofluorescent images of WGA staining of myocardia of the above mice (n = 6/group). Green represents WGA, blue represents DAPI, scale bars represent 20 μm. **L-M**, Statistical analyses of HW (**L**) and HW/TL (**M**) of the above mice (n = 6/group). **N**, Statistical analysis of myocyte cross section area of the WGA staining of the above mice (n = 6/group). Data are expressed as mean ± SEM. ns, not significant. $^{*}P < 0.05$, $^{**}P < 0.01$, $^{***}P < 0.001$, $^{****}P < 0.0001$. Data in **B**, **C**, **D**, **E** and **F** were analyzed using multiple unpaired t tests. Data in **G**, **H**, **L**, **M** and **N** were analyzed using Student's t-test. (For interpretation of the references to color in this figure legend, the reader is referred to the Web version of this article.)

constructed by OBiO Biology (Shanghai, China). AAV packaging was conducted in accordance with our previous protocol [30]. In brief, 293AAV cells were co-transfected with the expression vectors and packaging vectors using a calcium phosphate-mediated protocol. Subsequently, after 72 h, the cells were harvested, and AAVs were purified utilizing cesium chloride (CsCl) gradient centrifugation. AAV9 was administered at a concentration of 1.0×10^{11} vg/mouse *via* tail vein injection.

2.5. Immunofluorescence staining

Bloods were flushed from the hearts using PBS containing 10 % potassium chloride, following which they were fixed in 4 % paraformaldehyde, embedded in paraffin, and sectioned into 6-μm thick slices. The samples were then blocked with 5 % bovine serum albumin for 1 h at room temperature, and subsequently incubated with primary antibodies against Wheat Germ Agglutinin (abcam, ab178444) overnight at 4 °C. Following this, the samples were exposed to a secondary antibody against rabbit IgG H&L (Alexa Fluor® 488) (abcam, ab150077) for 1 h at room temperature. Nuclei were stained with DAPI, and images were captured using a fluorescence microscope. The cross-sectional area of cardiomyocytes in 5 randomly selected high-power fields (400 ×) within each section was measured using ImageJ software (National Institutes of Health, Bethesda, MD, USA).

2.6. Oil red O staining

4 % paraformaldehyde was used to fix frozen sections (10-μm-thick) of the myocardial tissues or neonatal mouse cardiomyocytes (NMCMs). Lipids in cardiomyocytes were stained with 0.5 % Oil red O (Sigma-Aldrich, O0625, St. Louis, MO, USA) in 60 % isopropanol. Oil red O dye that was not bound in cardiomyocytes was removed with 60 % isopropanol [28]. Subsequently, the nuclei were stained with hematoxylin, followed by sealing with Glycerol Jelly Mounting Medium (Beyotime, C0187, Shanghai, China). Images were captured using an optical microscope. In the case of NMCMs, absolute isopropanol was used to extract the stained Oil red O dye, and the optical density of the extracted dye was measured at 540 nm [28]. For tissue sections, the Oil red O area of 5 randomly selected high-power fields (200 ×) within each section was analyzed using ImageJ software (National Institutes of Health, Bethesda, MD, USA).

2.7. Transmission electron microscopy

Upon completion of the intervention, ventricles (1 mm^3) of the mice were fixed in 2.5 % glutaraldehyde in 0.1 M cacodylate buffer (Servicebio®, G1102, Hubei, China), followed by incubation in 2 % osmium tetroxide (Sigma-Aldrich) and 1 % aqueous uranyl acetate (Sigma-Aldrich) [28]. Subsequently, the samples underwent dehydration through a series of graded ethanol incubations and were embedded in epoxy resin (Sigma-Aldrich) [28]. The 60–80 nm ultrathin sections were cut using an ultra-microtome (Ultra 45°, Daitome) and double-stained with uranyl acetate (Sigma-Aldrich) and lead citrate (Sigma-Aldrich) [28]. The ultrastructure was examined using a transmission electron microscope (HT7700, Hitachi Ltd, Ohta, Japan) at 80 kV [28]. Lipid droplets were identified as electron-translucent structures lacking a surrounding membrane and were quantitatively analyzed in 10 randomly selected fields (× 6.0k) using ImageJ software (National Institutes of Health, Bethesda, MD, USA). Mitochondrial morphology was estimated using a 5-grade scoring system as described in a previous publication [31]. A score of 4 indicated cristae content >80 %, with well-defined and intact cristae [31]. A score of 3 denoted cristae content ranging from 60 % to 80 %, with slightly irregular cristae [31]. A score of 2 represented cristae content between 30 % and 60 %, characterized by major distortions and discontinuous membranes and cristae [31]. A score of 1 indicated cristae content between 10 % and 30 %, with severely fragmented or swollen cristae and warped membranes [31]. Finally, a score of 0 signified cristae content <10 %, with severely broken membranes and almost absent cristae [31].

2.8. GTT and ITT

Upon completion of the intervention, the mice underwent a fasting period of 12–16 h, followed by intraperitoneal injection with 1 g/kg D-(+)-Glucose (Sigma-Aldrich, G7021) for GTT or 1U/kg insulin (Novo Nordisk A/S, Novolin® R, Copenhagen, Denmark) for ITT. Blood glucose levels of the mice were assessed using a glucometer (OneTouch®, OneTouch Verio Vue®, NJ, USA) at 0, 30, 60, and 120 min post-injection. GraphPad Prism software (Version 9.0.0, San Diego, CA, USA) was utilized to plot the blood glucose curve at different time points and calculate the area under the curve (AUC).

2.9. Serum measurement

Upon completion of the intervention, blood samples were obtained from the eye sockets of the mice following a 12-h fast after sacrifice. These samples were allowed to clot at room temperature and then centrifuged to collect serum. The serum insulin concentrations were determined using a commercial Mouse Insulin (INS) ELISA Kit (CUSABIO, CSB-E05071 m, Hubei, China) in accordance with the manufacturer's protocol. Additionally, the serum concentrations of glucose, TG, total cholesterol (TC), high-density lipoprotein cholesterol (HDL-C), and low-density lipoprotein cholesterol (LDL-C) were assessed using commercial kits, including the Glucose Assay Kit (Rayto, S03039, Guangdong, China), TG Assay Kit (Rayto, S03027, Guangdong, China), TC Assay Kit (Rayto, S03042, Guangdong, China), HDL-C Assay Kit (Rayto, S03025, Guangdong, China), and LDL-C Assay Kit (Rayto, S03029, Guangdong, China) respectively. The homeostasis model assessment of insulin resistance (HOMA-IR) was calculated using the equation [Fasting blood glucose (FBG) (mmol/L) * Fasting insulin (FINS) (mIU/L)]/22.5, as per previous reports [32].

2.10. TG content

Upon completion of the intervention, cardiac tissues were excised from the mice and cryopreserved in liquid nitrogen. TG content in the heart tissues and NMCMs was assessed using a commercial TG Assay Kit (Nanjing Jiancheng Bioengineering Institute, A110-1-1, Jiangsu, China) and normalized by the protein concentration in accordance with the manufacturer's protocol.

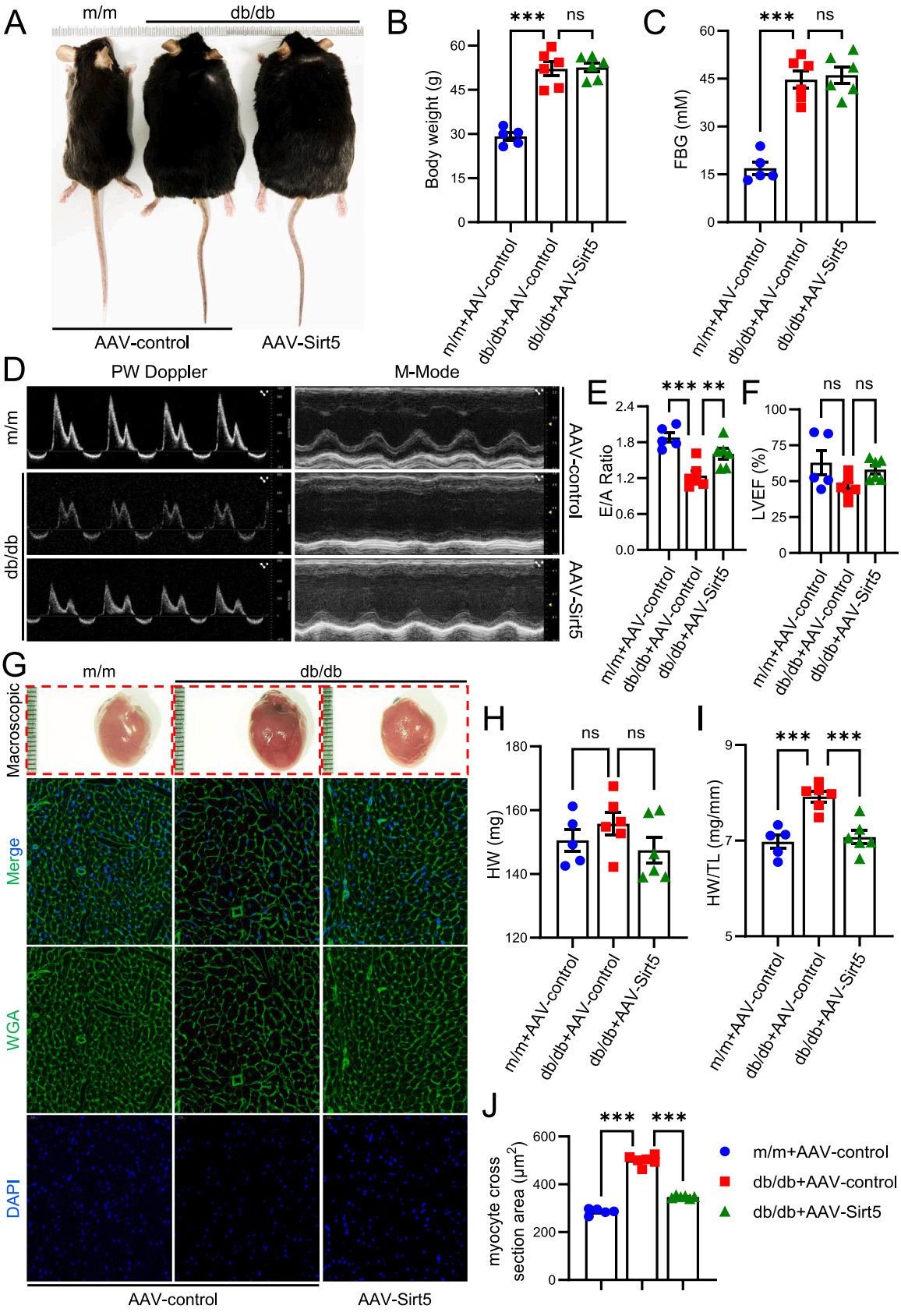

(caption on next page)

Fig. 3. Effects of *Sirt5* forced expression on cardiac function and hypertrophy in db/db mice. 20-week-old male m/m and db/db mice were infected with AAV9-*Sirt5* to force express *Sirt5* in cardiomyocytes, AAV9-control was used as control virus, cardiac function and hypertrophy were examined 8 weeks after infection. m/m + AAV-control: n = 5, db/db + AAV-control: n = 6, db/db + AAV-*Sirt5*: n = 6. **A**, Representative macroscopic images of the above mice. **B**, Statistical analysis of body weight of the above mice. **C**, Statistical analysis of FBG of the above mice. **D**, Representative echocardiographic images of PW Doppler (left) and M-Mode (right) of the above mice. **E-F**, Statistical analyses of E/A Ratio (**E**) and LVEF (**F**) of the above mice. **G**, Representative macroscopic images of hearts (*top row*) and immunofluorescent images of WGA staining of myocardia of the above mice. Green represents WGA, blue represents DAPI, scale bars represent 20 μm. **H–I**, Statistical analyses of HW (L) and HW/TL (M) of the above mice. **J**, Statistical analysis of myocyte cross section area of the WGA staining of the above mice. Data are expressed as mean ± SEM. ns, not significant. $^{**}P < 0.01$, $^{***}P < 0.001$. Data in **B**, **C**, **E**, **F**, **H**, **I** and **J** were analyzed using one-way ANOVA followed by Bonferroni post hoc analysis. (For interpretation of the references to color in this figure legend, the reader is referred to the Web version of this article.)

2.11. FA uptake measurement

For *in vivo* assessment, upon completion of the intervention, the mice were anesthetized with 80 mg/kg sodium pentobarbital *via* peritoneal injection. Subsequently, the mice received an injection of 1 μg/g BODIPY™ FL C_{16} (Invitrogen™, D3821) *via* their tail vein and were sacrificed 1 h later. Their hearts were excised and rinsed in PBS to swiftly remove residual blood. X-ray and fluorescence imaging were conducted using a small animal living fluorescence imaging system (In-Vivo Xtreme, Bruker, Germany), and the mean photons were analyzed using Bruker MI SE software (Version 7.2, Bruker, Germany). The detection parameters were set as follows: excitation wavelength 460 nm, emission wavelength 535 nm, and exposure time 2 s. For *in vitro* assessment, following treatment with palmitic acid (PA) or BSA, NMCMs were rinsed with PBS and cultured in 1 % BSA containing 50 μM BODIPY™ FL C_{16} at 37 °C for 30 min. Subsequently, the NMCMs were rinsed with 1 % BSA in PBS three times and fixed with 4 % paraformaldehyde at room temperature for 15 min. DAPI was utilized to stain the nucleus. Images were captured using a fluorescence microscope and analyzed using ImageJ software (National Institutes of Health, Bethesda, MD, USA).

2.12. Cardiac FAO measurement

Upon completion of the intervention, adult mouse cardiomyocytes (AMCMs) were isolated from the mice using Langendorff according to a previously reported protocol. The AMCMs were seeded in a Seahorse XF96 Culture Microplate (Agilent, 101085-004) and cultured with XF Assay Medium Modified DMEM (Seahorse Bioscience, 103680-100) containing 0.5 mM glucose, 1 × GlutaMAX (Gibco™, 35050079), and 0.5 mM Carnitine (Sigma-Aldrich, 8.40092) overnight. The medium was then replaced with FAO assay medium (111 mM NaCl, 4.7 mM KCl, 1.25 mM $CaCl_2$, 2.0 mM $MgSO_4$, 1.2 mM $Na2HPO_4$, 2.5 mM glucose, 0.5 mM carnitine, and 5 mM HEPES) at 37 °C for 30 min prior to the start of the assay. Palmitate-BSA (200 μM, Sigma-Aldrich, P0500) or BSA (34 μM, Sigma-Aldrich, 126575) was added to the medium. The OCR was measured by hydrated probes in the Agilent Seahorse Xfe96 Extracellular Flux Analyzer at baseline and after the injection of oligomycin (1 μM, MCE, HY-N6782, Montclair, NJ, USA), carbonyl cyanide 4-(trifluoromethoxy) phenylhydrazone (FCCP, 1 μM, MCE, HY-100410), and antimycin A (0.5 μM, Sigma-Aldrich, A8674). Total protein was then extracted with Cell Lysis Buffer (CST, #9803) and quantified using the BCA Protein Quantitation Kit (Shenergy Biocolors, K3000, Shanghai, China). The OCR values were normalized by the protein concentration.

2.13. Widely targeted metabolomics

Upon completion of the study, heart tissues from both WT (n = 4) and *Sirt5*$^{-/-}$ (n = 3) mice, which were treated with HFD/STZ, were excised after sacrifice and sent to PTM Biolabs Inc (Zhejiang, China) for widely targeted metabolomics analysis. In brief, the heart tissues were homogenized and combined with 70 % methanol containing internal standard extract. The mixture was then centrifuged, and the supernatant was stored in a −20 °C refrigerator overnight. Subsequently, the supernatant was centrifuged again and transferred to the liner of the corresponding injection bottle for on-board analysis. The sample extracts were analyzed using a LC-ESI-MS/MS system (UPLC, ExionLC AD, https://sciex.com.cn/; MS, QTRAP® System, https://sciex.com/) [33]. LIT and triple quadrupole scans were acquired on a triple quadrupole-linear ion trap mass spectrometer (QTRAP), QTRAP® LC-MS/MS System, equipped with an ESI Turbo Ion-Spray interface, operating in positive and negative ion mode and controlled by Analyst 1.6.3 software (Sciex) [33]. A specific set of MRM transitions were monitored for each period according to the metabolites eluted within this period.

Unsupervised principal component analysis (PCA) was conducted using the "prcomp" package within R. Prior to the unsupervised PCA, the data was unit variance scaled [34]. The results of the hierarchical cluster analysis (HCA) for both samples and metabolites were visualized as heatmaps with dendrograms [34]. Additionally, Pearson correlation coefficients (PCC) between samples were calculated using the cor function in R and presented as heatmaps [34]. Both HCA and PCC analyses were performed using the R package ComplexHeatmap [34]. For the HCA, normalized signal intensities of metabolites (unit variance scaling) were represented as a color spectrum [34]. Significantly regulated metabolites between groups were identified based on variable importance in projection (VIP) values ≥ 1 and absolute Log2FC ≥ 1 [34]. VIP values were extracted from the orthogonal partial least squares-discriminant analysis (OPLS-DA) result, which also included score plots and permutation plots, and was generated using the R package MetaboAnalystR [34]. The data was log-transformed (log2) and mean-centered prior to OPLS-DA [34]. To prevent overfitting, a permutation test (200 permutations) was conducted [34].

2.14. 4D label-free relative quantitative proteomics and succinylomics

Upon completion of the study, heart tissues were excised from WT (n = 6) and *Sirt5*$^{-/-}$ (n = 6) mice, all of which were treated with HFD/STZ. These tissues were combined into one sample to ensure sufficient protein content in each group, and subsequently sent to PTM Biolabs Inc (Zhejiang, China) for 4D label-free proteomics and succinylome analyses. In brief, the heart tissues were homogenized in liquid nitrogen and lysed in a lysis buffer (8 M urea, 1 % Protease Inhibitor Cocktail, 3 μM TSA, and 50 mM nicotinamide). The protein concentration was determined using the BCA kit. Equivalent proteins from each group were precipitated by 20 % trichloroacetic acid, washed with acetone, sonicated with 200 mM triethylammonium bicarbonate, and then digested with trypsin. Samples were reduced with 5 mM Dithiothreitol and alkylated with 11 mM Iodoacetamide. Affinity enrichment of succinylated peptides was performed using agarose beads-conjugated pan *anti*-succinyllysine antibody (PTM BIO, PTM-402). The bound peptides were eluted from the agarose beads by 0.1 % trifluoroacetic acid. The eluted fractions were combined and vacuum-dried, and then desalted with C18 ZipTips (Millipore, ZTC18 M). The peptides were dissolved in solvent A and separated in the NanoElute UPLC system. Subsequently, the peptides were subjected to NSI source followed by tandem mass spectrometry (MS/MS) in timsTOF Pro coupled online to the UPLC. Both the peptide precursor and its secondary fragments were detected and analyzed using TOF. The *m/z* scan range was 100-1700 for full scan, and the parallel accumulation serial fragmentation (PASEF) mode was set for data acquisition. The resulting MS/MS data were processed using the Maxquant search engine (v1.6.6.0). Tandem mass spectra were searched against the Mouse uniprot database concatenated with a reverse decoy database, and proteins

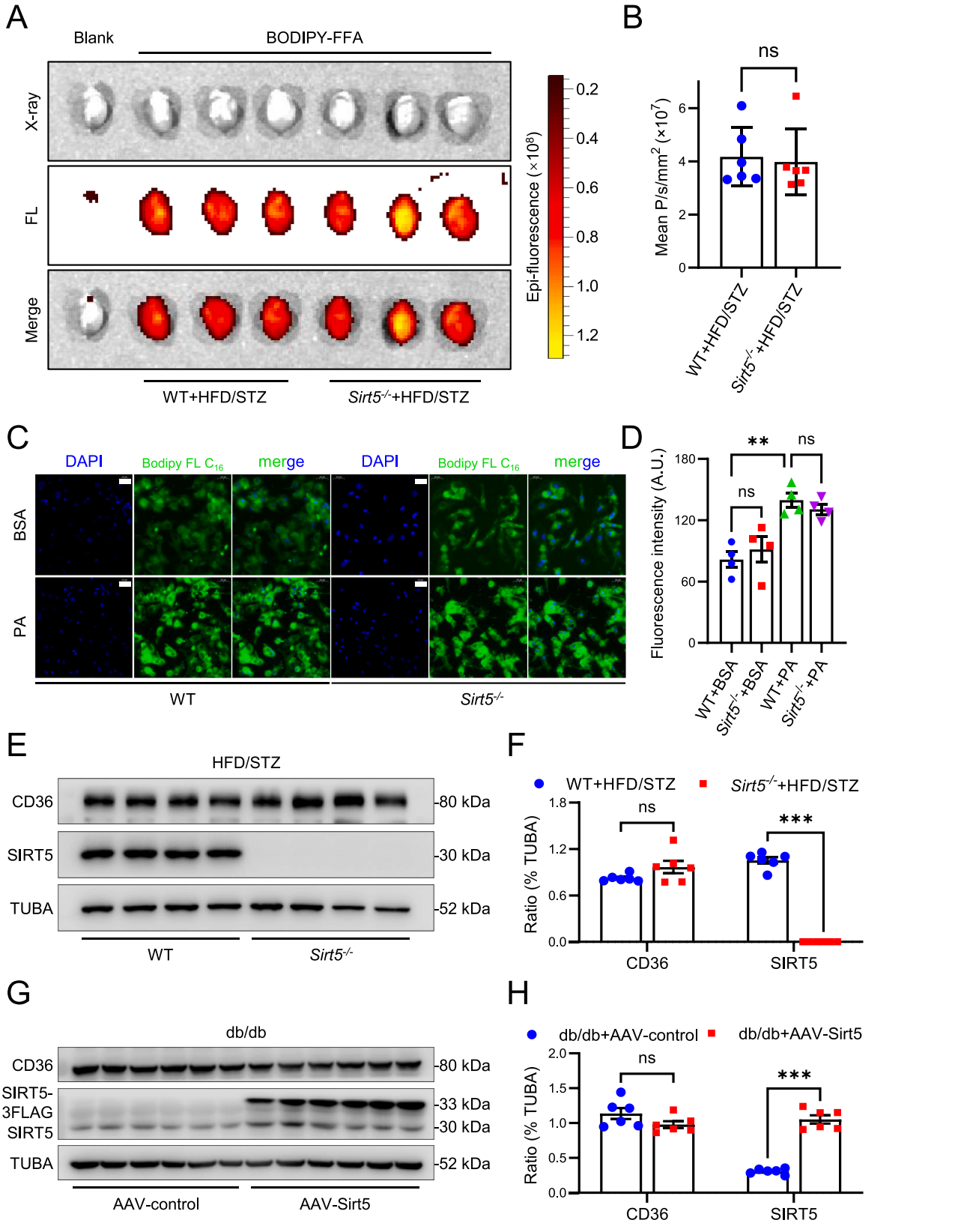

(caption on next page)

Fig. 4. Effects of *Sirt5* on FA uptake in diabetic mice and PA-treated NMCMs. A, Representative X-ray and fluorescent images of cardiac BODIPY™ FL C_{16} uptake in WT and *Sirt5*$^{-/-}$ mice after HFD/STZ induction (n = 6/group). FL: Fluorescence. **B**, Statistical analysis of epi-fluorescence of X-ray and fluorescent images of the above mice. **C**, Representative fluorescent images of Bodipy™ FL C_{16} uptake in WT and *Sirt5*$^{-/-}$ NMCMs treated with BSA or 200 μM PA for 48 h (n = 4/group). Green: Bodipy™ FL C_{16}. Blue: DAPI. Scale bars: 20 μm. **D**, Statistical analysis of fluorescence intensity of the fluorescence images of the above NMCMs. **E**, Representative Western blot of myocardial FA transporter CD36 protein expression in WT and *Sirt5*$^{-/-}$ mice after HFD/STZ induction (n = 6/group), TUBA (α-tubulin) was used as the loading control. **F**, Statistical analysis of the Western blot. **G**, Representative Western blot of myocardial CD36 protein expression in db/db mice transfected with AAV9-control or AAV9-*Sirt5* (n = 6/group), TUBA (α-tubulin) was used as the loading control. **H**, Statistical analysis of the Western blot. Data are expressed as mean ± SEM. ns, not significant, $^{**}P < 0.01$, $^{***}P < 0.001$, $^{****}P < 0.0001$. Data in **B** was analyzed using Student's t-test. Data in **D** was analyzed using one-way ANOVA followed by Bonferroni post hoc analysis. Data in **F** and **H** was analyzed using multiple unpaired t tests. (For interpretation of the references to color in this figure legend, the reader is referred to the Web version of this article.)

and peptide spectrum matches (PSMs) were identified with a 1 % FDR.

The differentially succinylated proteins encompassed those exhibiting an increase of more than 2-fold in *Sirt5*$^{-/-}$ + HFD/STZ compared with WT + HFD/STZ, as well as those exclusively detected in *Sirt5*$^{-/-}$ + HFD/STZ. Subcellular localization of the differentially succinylated proteins was predicted using Wolfpsort software. Furthermore, the differentially succinylated proteins were annotated using KEGG online service tools KAAS and subsequently mapped onto the KEGG pathway database using KEGG online service tools KEGG mapper. Targeted functional proteins of *Sirt5* in regulating FAO were identified based on their succinylation ratio, whether they function as rate-limiting enzymes, and through integrated analysis with results from the widely targeted metabolomics.

2.15. Immunoprecipitation (IP) and western blotting

Upon completion of the study, total protein was extracted from the heart tissues of the mice using Pierce™ IP Lysis Buffer (Thermo Scientific, 87788) containing EDTA-free protease inhibitor cocktail (abcam, ab201111), nicotinamide (50 mM; Sigma-Aldrich, N3376), and trichostatin A (3 μM; Selleck, S1045). Protein concentrations were quantified using the BCA Protein Quantitation Kit (Shenergy Biocolors, K3000). For IP, 2 mg of protein was incubated with primary antibodies against CPT2 (Proteintech, 26555-1-AP, Chicago, IL, USA) overnight at 4 °C. The antibody-antigen complex was then immunoprecipitated using Pierce™ Protein A/G Magnetic Beads (Thermo Scientific, 88802) and eluted with 1 × Pierce™ Lane Marker Non-Reducing Sample Buffer (Thermo Scientific, 39001). The eluted samples or 3 % input were resolved on SDS-PAGE gels and subsequently blotted onto 0.2 μm PVDF membranes. The membranes were probed with primary antibodies against Ksuc (PTM BIO, PTM-401), *Sirt1* (CST, 2314), *Sirt2* (CST, 12650), *Sirt3* (CST, 5490), *Sirt4* (CST, 24662), *Sirt5* (CST, 8782), *Sirt6* (CST, 12486), *Sirt7* (CST, 5360), CPT2, or TUBA (CST, 2144) overnight at 4 °C, and then incubated with horseradish peroxidase-linked secondary antibodies against rabbit IgG (CST, 7074), mouse IgG (CST, 7076), or conformation-specific rabbit IgG (CST, 5127) for 1 h at room temperature. Immunoblots were detected using an ECL system (Merck Millipore, WBULS0500). The intensity of bands was quantified with Image J (National Institutes of Health, Bethesda, MD, USA) and normalized to the control.

2.16. NMCMs isolation and PA treatment

NMCMs were enzymatically isolated from the ventricles of WT and *Sirt5*$^{-/-}$ mice aged 1–3 days, following previously established protocols [28]. In brief, ventricles were excised from neonatal mice and digested with 0.1 % trypsin (Gibco™, 15050065) in D-hanks buffer at 4 °C overnight. Subsequently, the ventricles underwent three cycles of digestion with collagenase II (Gibco™, 17101015) in D-hanks buffer at 37 °C for 10 min per cycle. NMCMs were collected from each cycle and purified using a differential-speed adherence method. Cytosine-B-D-arabino-furanoside hydrochloride (Sigma-Aldrich, C6645) was added to the culture medium to inhibit the proliferation of non-cardiomyocytes. The NMCMs were starved with fetal bovine serum-free medium overnight and then treated with BSA (control) or PA (200 μM) for 48 h, followed by harvest for analyses.

2.17. Adenovirus construction and transfection

We utilized adenovirus to overexpress *Sirt5*, *Cpt2-WT*, or *Cpt2-K424R* in NMCMs for *in vitro* studies and in myocardia for *in vivo* studies. *Ad-Sirt5*, *Ad-control*, *Ad-6His-Cpt2-WT*, and *Ad-6His-Cpt2-K424R* were synthesized and constructed by OBiO Biology (Shanghai, China). The AdMax system was employed to package the adenovirus, following our previous protocol [28]. In brief, AD293 cells were transfected with expression vectors and packaging vectors simultaneously using a calcium phosphate-mediated protocol. After 72 h, the cells were harvested, and the adenovirus was purified using CsCl gradient centrifugation. *Ad-Sirt5*, *Ad-control*, *Ad-6His-Cpt2-WT*, and *Ad-6His-Cpt2-K424R* were used at a MOI of 100 for transfecting NMCMs. *Ad-6His-Cpt2-WT* and *Ad-6His-Cpt2-K424R* were administered at a concentration of 1×10^9 vg/mouse *via* tail vein injection.

2.18. CPT2 activity measurement

CPT2 activity in NMCMs and myocardia from the mice was assessed following established procedures [35]. In brief, NMCMs or myocardia were homogenized with lysis buffer (10 mM HEPES, pH7.4; 0.1 % Triton X-100; 11.5 % (w/v) sucrose; 5 % (v/v) protease inhibitor cocktail) and centrifuged at 1500×*g* at 4 °C for 5 min. The supernatant was collected and added to the reaction buffer (200 mM HEPES, 10 mM EGTA, 0.2 M sucrose, 400 mM KCl, 2 mM DTNB, 0.13 % (w/v) bovine serum albumin, 20 μM palmityl-CoA, 10 μM malonyl-CoA), and incubated for 1 h at 25 °C. The reaction was initiated by adding 15 mM L-carnitine and measured using a spectrophotometer. Total protein was quantified using a BCA Protein Quantitation Kit (Shenergy Biocolors, K3000). The CPT2 activity was determined as μmol/h/mg prot.

2.19. Statistical analysis

Data were presented as mean ± SEM. Comparisons of two groups were analyzed by Student's t-test. Comparisons of multiple groups were analyzed by one-way ANOVA, followed by Bonferroni post hoc analysis. All statistical analyses were performed using the GraphPad Prism Software (San Diego, CA, USA). *P*-values less than 0.05 were considered statistically significant.

3. Results

3.1. Sirt5 is the only sirtuin gene altered in myocardia from diabetic HF patients

In order to ascertain the changes in sirtuins expressions during the development of DbCM, we obtained a diabetic HF-related expression profiling microarray (GSE26887) from the GEO repository and conducted an analysis using log2 GC-RMA signal. The dataset comprised LV cardiac biopsies from five control non-HF patients and seven diabetic HF patients, with gene expression assessed using the Affymetrix GeneChips Human Gene 1.0 ST array. As depicted in Fig. 1A, only the expression of *Sirt5* exhibited a modestly upregulation in diabetic HF patients, while no

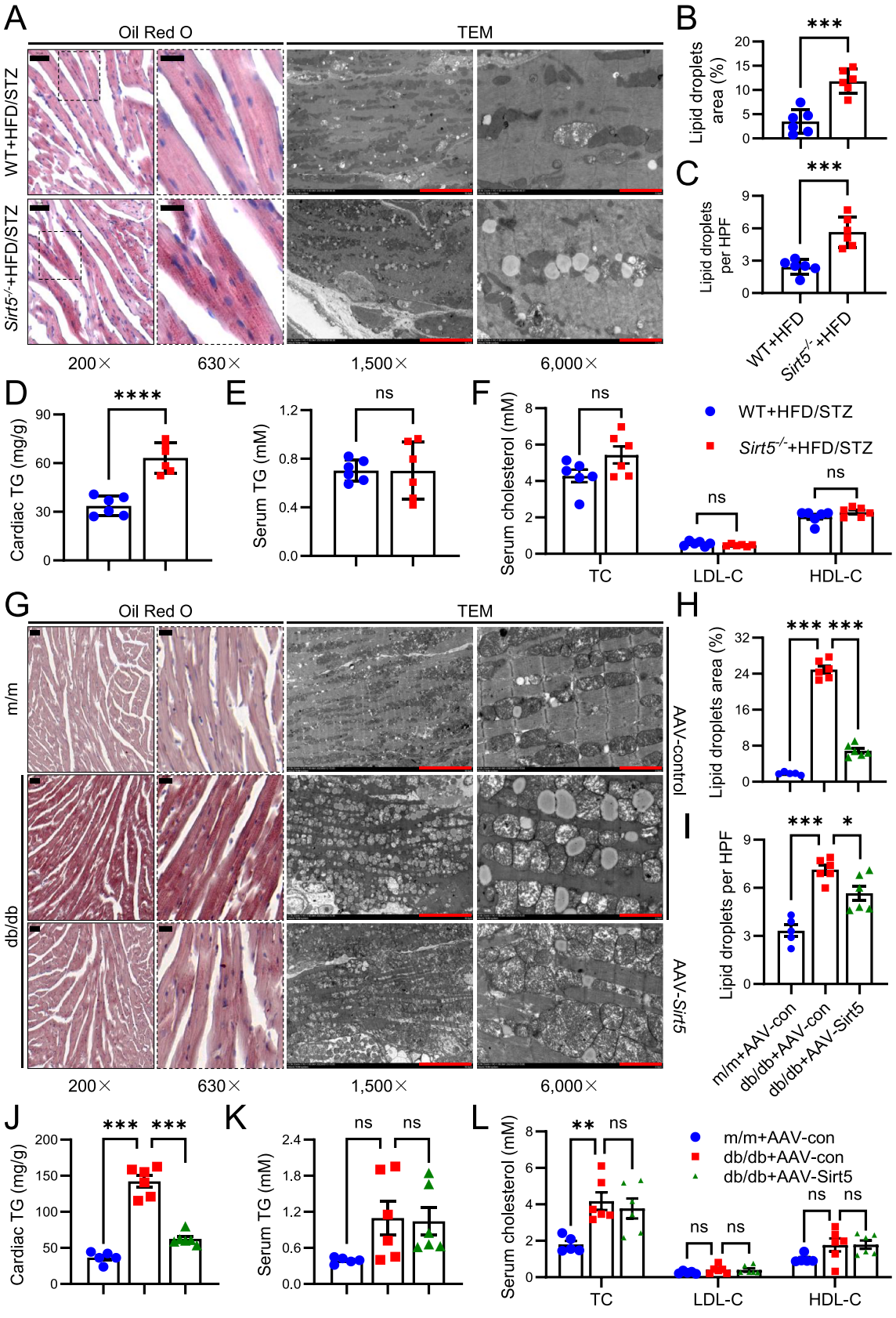

(caption on next page)

Fig. 5. Effects of *Sirt5* knockout or *Sirt5* forced expression on cardiac lipotoxicity in diabetic mice. A, Representative images of myocardial Oil red O staining (*left*) and TEM (*right*) in WT and *Sirt5*$^{-/-}$ mice after HFD/STZ induction (n = 6/group). Scale bar (*left*): 50 μm (200 ×) or 20 μm (630 ×). Scale bar (*right*): 10 μm (1500 ×) or 2 μm (6000 ×). **B–C**, Statistical analyses of lipid droplets area in Oil red O staining (**B**) and lipid droplets per HPF in TEM (**C**) in the above mice (n = 6/group). **D-F**, Statistical analyses of cardiac TG content (**D**), serum TG concentration (**E**) and serum cholesterols concentration (including TC, LDL-C and HDL-C) (**F**) of the above mice (n = 6/group). **G**, Representative images of myocardial Oil red O staining (*left*) and TEM (*right*) in the diabetic mice transfected with AAV9-control or AAV9-*Sirt5*. Scale bar (*left*): 50 μm (200 ×) or 20 μm (630 ×). Scale bar (*right*): 10 μm (1500 ×) or 2 μm (6000 ×). **H–I**, Statistical analyses of lipid droplets area in Oil red O staining (**H**) and lipid droplets per HPF in TEM (**I**) in the above mice. **J-L**, Statistical analyses of cardiac TG content (**J**), serum TG concentration (**K**) and serum cholesterols concentration (including TC, LDL-C and HDL-C) (**L**) of the above mice. Data are expressed as mean ± SEM. ns, not significant, $^{*}P < 0.05$, $^{**}P < 0.01$, $^{***}P < 0.001$, $^{****}P < 0.0001$. Data in **B-E** were analyzed using Student's t-test. Data in **F** was analyzed using multiple unpaired t tests. Data in **H–K** was analyzed using one-way ANOVA followed by Bonferroni post hoc analysis. Data in L was analyzed using two-way ANOVA followed by Tukey's post hoc analysis. (For interpretation of the references to color in this figure legend, the reader is referred to the Web version of this article.)

discernible alteration could be observed in the expression of other sirtuins.

To further validate these results, we used 32-week-old db/db mice as the model for DbCM and assessed cardiac sirtuins. Consistent with the results found in human data, the cardiac protein expression of *Sirt5* was indeed upregulated in db/db mice compared to m/m control mice (Fig. 1B and C). Conversely, no significant difference in the protein expression of other sirtuins could be observed between the m/m mice and db/db mice (Fig. 1B and C). These findings showed that *Sirt5* was significantly upregulated in diabetic heart.

3.2. *Sirt5 is an important regulator of cardiac function and structure in diabetic mice*

To investigate the role of *Sirt5* in DbCM, both WT mice and *Sirt5*$^{-/-}$ mice were subjected to low-dose STZ injections for 5 consecutive days and maintained on a HFD for 24 weeks to induce DbCM. The absence of *Sirt5* did not result in compensatory expression of other sirtuins in the diabetic heart (Figs. S1A–S1B). Both WT and *Sirt5*$^{-/-}$ mice exhibited significant increase in body weight and FBG due to HFD/STZ (Figs. S2A–S2B). However, the knockout of *Sirt5* did not affect body weight or FBG during HFD/STZ induction (Figs. S2A–S2B). Subsequently, we assessed whether *Sirt5* regulates glucose tolerance and insulin resistance. As depicted in Figs. S2C–S2F, no difference was observed in GTT and ITT between WT and *Sirt5*$^{-/-}$ mice following HFD/STZ induction. Furthermore, the absence of *Sirt5* did not appear to influence serum insulin contents or HOMA-IR in the mice (Figs. S2G–S2H). These findings indicated that *Sirt5* did not play a regulatory role in glucose metabolism in DbCM.

To further elucidate the role of *Sirt5* in DbCM, we conducted echocardiography and histological analyses. Following HFD/STZ induction, *Sirt5*$^{-/-}$ mice exhibited a more pronounced decrease in E/A ratio, e', and dp/dt_{min}, along with a more obvious increase in the E/e' ratio compared to WT mice (Fig. 2A–D and 2G), indicating a deterioration in diastolic dysfunction. Additionally, while no disparity was observed in LVEF and LVFS between WT and *Sirt5*$^{-/-}$ mice, dp/dt_{max} was significantly reduced in *Sirt5*$^{-/-}$ mice (Fig. 2A, 2E-2F and 2H), suggesting the presence of systolic dysfunction. Compared with the WT mice, more significant increases in HW and HW/TL ratio could be observed in *Sirt5*$^{-/-}$ mice following HFD/STZ induction (Fig. 2I–J and 2L-2M). Consistent with these findings, WGA staining demonstrated an augmentation in myocyte cross-sectional area in *Sirt5*$^{-/-}$ mice compared to WT mice (Fig. 2K and N). Collectively, these results indicated that the deficiency of *Sirt5* exacerbated cardiac dysfunction and hypertrophy in HFD/STZ-induced DbCM, independent of blood glucose and insulin resistance.

Given the significant effect of *Sirt5* deficiency on DbCM development, we next sought to verify whether forced expression of *Sirt5* could protect against DbCM. AAV9 was used to mediate cardiac-specific forced expression of *Sirt5* in db/db mice. In comparison with m/m mice, greater weight gain and higher fasting blood glucose levels were observed in db/db mice, while cardiac *Sirt5* overexpression had no significant effect on weight gain and fasting blood glucose levels in db/db mice (Fig. 3A–C). Forced expression of *Sirt5* significantly correct the diastolic dysfunction of db/db mice, as showed by improved E/A ratio (Fig. 3D and E). Meanwhile, no significant difference in systolic function was observed among m/m mice, db/db mice, and *Sirt5*-forced expressed db/db mice (Fig. 3D and F). HW and the HW/TL ratio were also significantly corrected by cardiac *Sirt5* expression in db/db mice (Fig. 3G–I). WGA staining showed that the increase in myocyte cross-sectional area in db/db mice was attenuated by cardiac *Sirt5* forced expression (Fig. 3G and J). These data indicate that forced cardiac *Sirt5* expression alleviates diastolic dysfunction and hypertrophy in DbCM.

Taken together, gain- and loss-of-function evidence clarify *Sirt5* as a pivotal determinant of cardiac function and hypertrophy in the development of DbCM.

3.3. *Cardiac lipotoxicity is exacerbated by Sirt5 knockout but attenuated by Sirt5 forced expression in DbCM*

Considering that cardiac lipotoxicity is a pivotal pathogenic factor of DbCM, we therefore further investigate the impact of *Sirt5* on ectopic fat deposition in cardiomyocytes. Firstly, FFA uptakes were examined both *in vivo* and *in vitro*. As depicted in Fig. 4A and B, no discernible difference was observed in the uptake of BODPY-FA by heart between the WT mice and *Sirt5*$^{-/-}$ mice after HFD/STZ induction. Similar results were obtained in PA-induced lipotoxicity in cardiomyocytes (Fig. 4C and D). Furthermore, CD36, the FA transporter in cardiomyocytes responsible for mediating cardiac lipid uptake in DbCM, exhibited comparable protein expression levels between WT and *Sirt5*$^{-/-}$ mice following HFD/STZ (Fig. 4E and F), as well as between control and *Sirt5* forced expression db/db mice (Fig. 4G and H). Taken together, these results showed that *Sirt5* does not affect FFA uptake in cardiomyocytes.

Next, we further examine the function of *Sirt5* on lipid deposition in cardiomyocytes. *In vivo*, Oil red O staining revealed a greater accumulation of lipid droplets in the myocardium of *Sirt5*$^{-/-}$ mice compared to WT mice following HFD/STZ induction (Fig. 5A and B). Similarly, TEM demonstrated that the absence of *Sirt5* resulted in increased deposition of lipid droplets in cardiomyocytes compared to WT (Fig. 5A and C). Given that cardiomyocytes are weak in FA synthesis and mainly rely on the uptake it from the blood circulation, we subsequently investigated the effect of *Sirt5* on the lipid profiles. As depicted in Fig. 5D, *Sirt5* knockout significantly elevated cardiac TG content compared to WT following HFD/STZ induction. However, the serum lipid profiles, including TG, TC, LDL-C, and HDL-C, remained similar between WT mice and *Sirt5*$^{-/-}$ mice after HFD/STZ induction (Fig. 5E and F). *In vitro*, PA was utilized to induce cardiomyocytes lipotoxicity to model DbCM. Corroborating the *in vivo* findings, Oil red O staining demonstrated that the absence of *Sirt5* significantly enhanced PA-induced lipid droplet deposition and increased TG contents (Figs. S3A–S3D). Therefore, these data indicated that the deficiency of *Sirt5* exacerbated cardiac lipotoxicity in DbCM, potentially contributing to cardiac dysfunction and hypertrophy.

We proceeded to validate the impact of *Sirt5* forced expression on cardiac lipids deposition during DbCM. *In vivo*, Oil red O staining revealed a greater accumulation of lipids in the myocardium of db/db mice compared with m/m mice, which was significantly reduced by cardiac *Sirt5* forced expression in the db/db mice (Fig. 5G and H).

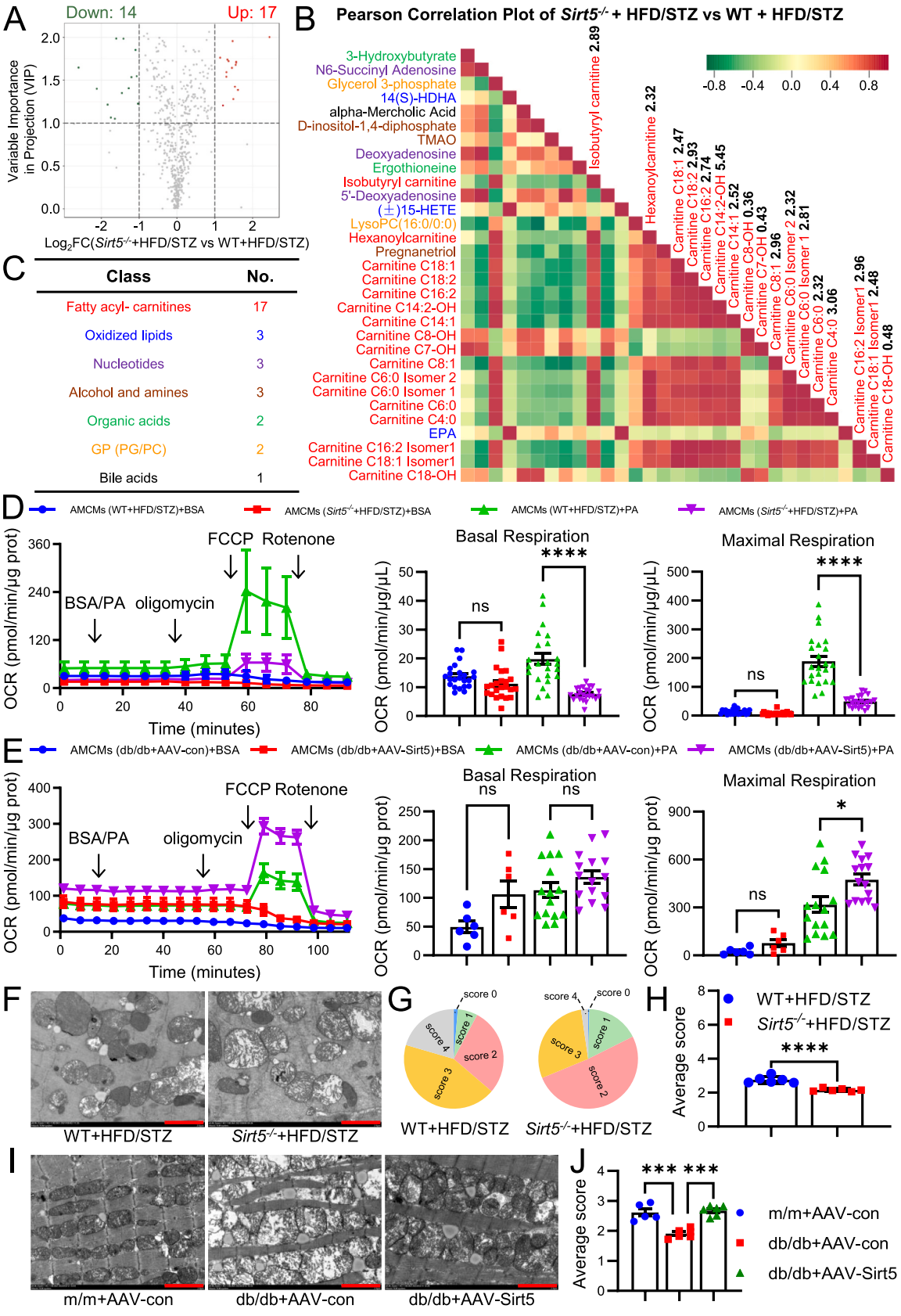

(caption on next page)

Fig. 6. Effects of *Sirt5* on cardiac FAO and mitochondrial integrity in diabetic mice. A-C, Widely targeted metabolomics of myocardia in WT (n = 3) and *Sirt5*$^{-/-}$ (n = 4) mice after HFD/STZ induction. **A**, Volcano plot of the metabolomics. **B**, Pearson correlation plot of the differential metabolites of the metabolomics. Metabolites are ordered according to correlation coefficient. Correlations between each pair of metabolites are displayed in the cells of the heatmap. Cells are color coded with colors ranging from green to red to depict correlations ranging from −1 to 1. **C**, Classification of the differential metabolites of the metabolomics. **D**, Seahorse metabolic analysis of FAO of AMCMs, that were isolated from WT and *Sirt5*$^{-/-}$ mice after HFD/STZ induction (n = 6/groups, 3–4 wells/mouse), at the presence of BSA or PA. **E**, Seahorse metabolic analysis of FAO of AMCMs, that were isolated from db/db mice transfected with AAV9-*control* or AAV9-*Sirt5* (n = 3/groups, 2–5 wells/mouse), at the presence of BSA or PA. **F**, Representative images of myocardial TEM in WT and *Sirt5*$^{-/-}$ mice after HFD/STZ induction (n = 6/group). Scale bar: 2 μm (6000 ×). **G**, Pie chart shows the prevalence of the individual score grades across the analyzed mitochondrial population in myocardia from WT and *Sirt5*$^{-/-}$ following HFD/STZ induction. **H**, Bar graph shows the overall mean scores in each group (n = 6/group). **I**, Representative images of myocardial TEM in m/m mice and db/db mice transfected with AAV9-*control* or AAV9-*Sirt5*. Scale bar: 2 μm (6000 ×). **J**, Bar graph shows the overall mean scores in each group (n = 5–6/group). Data are expressed as mean ± SEM. ns, not significant, *$P < 0.05$, ***$P < 0.001$, ****$P < 0.0001$. Data in **D-E** and **J** was analyzed using one-way ANOVA followed by Bonferroni post hoc analysis. Data in **H** was analyzed using Student's t-test. (For interpretation of the references to color in this figure legend, the reader is referred to the Web version of this article.)

Similarly, TEM showed that less lipid droplets were deposited in cardiomyocytes in db/db mice transfected with AAV9-*Sirt5* compared with the control AAV9 (Fig. 5G and I). Although no significant influence on serum TG, TC, LDL-C, and HDL-C could be observed, cardiac *Sirt5* forced expression led to a reduction in cardiac TG levels (Fig. 5J–L). *In vitro*, adenovirus was used to force express *Sirt5* in cardiomyocytes. Oil red O staining showed that *Sirt5* forced expression significantly inhibited PA-induced lipid droplet deposition and the PA-induced increase in TG content in NMCMs (Figs. S3E–S3H). Therefore, these data indicated that forced expression of *Sirt5* alleviated cardiac lipotoxicity in DbCM.

To further dissect the function of *Sirt5* on cardiac lipids deposition, a widely targeted metabolomics analysis of the myocardia from the WT and *Sirt5*$^{-/-}$ mice after HFD/STZ induction was conducted. In this metabolomics study, a total of 614 metabolites were detected with a VIP≥1 in the myocardia of the mice, among which 17 metabolites were increased and 14 metabolites were decreased by more than 2-fold in *Sirt5*$^{-/-}$ mice compared with WT mice (Fig. 6A). More than a half (17/31) of the differential contents of metabolites were fatty acyl-carnitines, the majority of which were medium (C8–C12) and long (C14–C18)-chain fatty acyl-carnitines (Fig. 6B and C). Among the fatty acyl-carnitines, 14 were increased while only 3 were decreased by *Sirt5* knockout (Fig. 6B and C). Consistently, Pearson correlation plot showed that differential metabolites were significantly clustered in fatty acyl-carnitines (Fig. 6B). These data further indicated that *Sirt5* deficiency led to an accumulation of FA-derived intermediate metabolites in the diabetic heart.

Collectively, the aforementioned data indicated that *Sirt5* improves cardiac function and mitigated hypertrophy in DbCM by suppressing cardiac lipotoxicity. The accumulation of FA-derived intermediate metabolites in cardiomyocytes following *Sirt5* knockout could be attributed to insufficiency in FAO.

3.4. *Sirt5* increases cardiac FAO in DbCM

Considering that FA uptake was not affected by *Sirt5*, we proceeded to verify the effect of *Sirt5* on FAO in cardiomyocytes during DbCM. AMCMs were isolated from the WT and *Sirt5*$^{-/-}$ mice after HFD/STZ induction, or from the db/db mice that were transfected with AAV9-control or AAV9-*Sirt5*, followed by FAO measurement immediately after the attachment of AMCMs to the culture microplate. We found that both basal respiration and maximal respiration were significantly attenuated by *Sirt5* knockout in AMCMs isolated from the mice after HFD/STZ induction (Fig. 6D). Conversely, maximal respiration was significantly enhanced by *Sirt5* overexpression in AMCMs isolated from db/db mice (Fig. 6E). These data indicate a pivotal role of *Sirt5* in the regulation of cardiac FAO in DbCM. As mitochondria is the major organelles responsible for FAO in the context of DbCM, the sufficiency of FAO could serve as an indicator of mitochondrial function indirectly, which depends on the morphological integrity of the mitochondria. Therefore, we further investigated the effect of *Sirt5* on mitochondrial integrity in cardiomyocytes during DbCM. A five-grade scoring system, as per previous publications [31], was employed to evaluate mitochondrial morphology (Figs. S4A–S4B). As illustrated in Fig. 6F–H, the damage in mitochondrial morphology, characterized by swelling, distorted membranes, irregularities, and loss of cristae, was exacerbated by the deletion of *Sirt5* in mice following HFD/STZ induction, in comparison with WT. Conversely, forced expression of *Sirt5* significantly ameliorated diabetes-induced damage to mitochondrial morphology (Fig. 6I and J). Collectively, these findings indicated that *Sirt5* improved FAO, resulting in lipid accumulation in cardiomyocytes and cardiac lipotoxicity.

3.5. *Sirt5* regulates cardiac FAO and exacerbates lipotoxicity through Lys424 succinylation of CPT2

We next sought to elucidate the molecular mechanism of *Sirt5* in regulating FAO. Considering that *Sirt5* operates through the regulation of de-acylation of substrate proteins, our subsequent investigation involved the assessment of pan-acylation of cardiac proteins in WT and *Sirt5*$^{-/-}$ mice after HFD/STZ induction. As illustrated in Figs. S5A–S5B, lysine succinylation (Ksuc) exhibited the most significant increase, followed by lysine glutarylation, while lysine malonylation and acetylation showed no marked alterations in cardiac proteins between *Sirt5* knockout and WT heart. Building upon these findings, 4D label-free proteomics and succinylome analysis of the myocardia from WT and *Sirt5*$^{-/-}$ mice after HFD/STZ induction were conducted to identify the substrates of *Sirt5* in the regulation of FAO. Ksuc levels of 1698 peptides were found to be increased by more than 2-fold in *Sirt5*$^{-/-}$ mice compared with WT mice, and these were mapped to 549 unique proteins (Fig. 7A). The differentially succinylated proteins were predominantly located in mitochondria (Fig. 7B) and functionally enriched in fatty acid metabolism, including FAO, fatty acid elongation, and fatty acid biosynthesis (Fig. 7C).

An integrated analysis of widely targeted metabolomics, 4D label-free proteomics, and succinylomics were conducted to identify the potential substrate protein of *Sirt5* that regulates fatty acyl carnitine metabolism in the FAO pathway. As depicted in Fig. 7D and E, the Ksuc level in Lys424 residue of CPT2 was found to be increased nearly 340-fold in *Sirt5*$^{-/-}$ mice compared with WT mice after HFD/STZ induction, and this site was also identified as the top succinylated site in the succinylomics analysis. To validate this finding, myocardial CPT2 was immunoprecipitated from the mice and detected using a pan-succinylation antibody. Consistent with the succinylomics result, the Ksuc level of CPT2 was significantly increased in *Sirt5*$^{-/-}$ mice compared with WT mice after HFD/STZ induction (Fig. 7F and G). Consequently, the enzyme activity of CPT2 was found to be lower in the myocardia from *Sirt5*$^{-/-}$ mice compared with WT mice (Fig. 7H). Conversely, the Ksuc level of cardiac CPT2 was significantly reduced in db/db mice transfected with AAV9-*Sirt5* compared to the control AAV9 (Fig. S6A), resulting in an increase in the enzyme activity of CPT2 (Fig. S6B). Considering that CPT2 is critical for FAO, these data suggested that *Sirt5* deficiency might impair FAO and lead to the accumulation of fatty acyl-carnitines in diabetic mice by succinylating and inactivating CPT2.

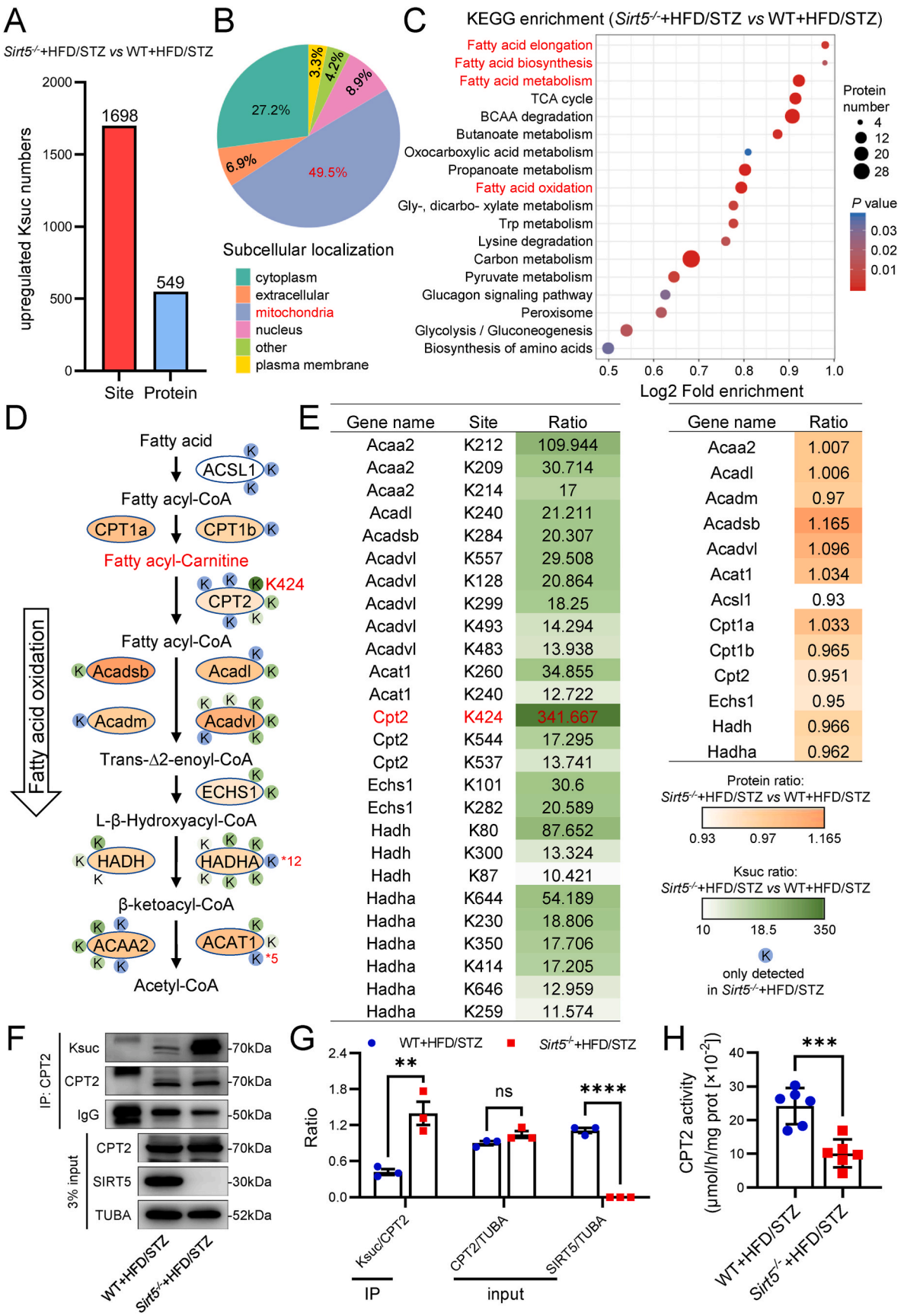

(caption on next page)

Fig. 7. Integrated analysis of the metabolomics and succinylomics identified CPT2 as the functional Ksuc substrate protein of *Sirt5* in regulating FAO. A-C, Bioinformatics analyses of the succinylomics in myocardia of the WT and *Sirt5*$^{-/-}$ mice after HFD/STZ induction. **A**, Number of succinylated peptides and proteins upregulated in myocardia of *Sirt5*$^{-/-}$ mice compared with WT mice after HFD/STZ induction. **B**, Subcellular localization of the differentially succinylated proteins. **C**, KEGG enrichment of the differentially succinylated proteins. **D**, Flow chart of integrated analysis of the differential Ksuc sites, Ksuc ratios and protein expression of metabolic enzymes and the differential metabolites in the FAO pathway. **E**, Tables of the differential Ksuc sites, Ksuc ratios (*left*) and protein expression (*Right*) of metabolic enzymes in the FAO pathway. **F**, Representative immunoprecipitation (IP) and Western blot of Ksuc and proteins expression levels of myocardial CPT2 in WT and *Sirt5*$^{-/-}$ mice after HFD/STZ induction (n = 3/group). TUBA was used as the loading control. Rabbit IgG was used as the IP control. **G**, Statistical analysis of the IP and Western blot. **H**, Statistical analysis of myocardial CPT2 activity in WT and *Sirt5*$^{-/-}$ mice after HFD/STZ induction (n = 6/group). Data are expressed as mean ± SEM. ns, not significant. $^{**}P < 0.01$, $^{***}P < 0.001$, $^{****}P < 0.0001$. Data in **G** and **H** was analyzed using Student's t-test.

Having identified Lys424 as the top succinylated site in the succinylomics analysis, our next objective was to ascertain whether Lys424 succinylation impacts the enzyme activity and molecular function of CPT2. The mass spectrum of succinylated Lys424 of CPT2 is presented in Fig. 8A, and further homology analysis revealed that Lys424 of CPT2 is highly conserved across different species (Fig. 8B). To investigate the effect of Lys424 de-succinylation on its enzyme activity, WT and *Sirt5*$^{-/-}$ mice were transfected with adenovirus *via* tail vein injection to overexpress His-tagged WT or K-to-R mutant (mimicking the de-Ksuc state) CPT2. One week after transfection, exogenous CPT2 was immunoprecipitated from the myocardia of the mice. As a result, the K424R mutant led to a significant reduction in the succinylation level of CPT2 compared with WT CPT2 in *Sirt5*$^{-/-}$ mice (Fig. 8C and D). Consistent with the alteration in succinylation level, the K424R mutant restored the enzyme activity of CPT2 that was inhibited by *Sirt5* deficiency (Fig. 8E). The K424R mutant also significantly increased maximal respiration compared with WT CPT2 in AMCMs from the *Sirt5*$^{-/-}$ mice (Fig. 8F), indicating that cardiac FAO was restored by Lys424 de-succinylation of CPT2 in *Sirt5*$^{-/-}$ mice. To further verify the effect of Lys424 de-succinylation on cardiac lipotoxicity, *Sirt5*$^{-/-}$ NMCMs were transfected with adenovirus to overexpress WT or K424R CPT2. As shown in Fig. 8G and H, forced expression of WT CPT2 was unable to inhibit PA-induced lipid deposition in *Sirt5*$^{-/-}$ NMCMs. In contrast, forced expression of the K424R mutant CPT2 significantly reduced lipid deposition in *Sirt5*$^{-/-}$ NMCMs that were treated with PA (Fig. 8G and H). In conclusion, *Sirt5* deficiency impaired cardiac FAO and exacerbated cardiac lipotoxicity in DbCM through Lys424 de-succinylation of CPT2.

4. Discussion

Excessive FA and FA-derived metabolites inside cardiomyocytes are the primary pathogenic factor contributing to cardiac lipotoxicity in DbCM, but the way to reduce them and thus mitigate DbCM are not well elucidated. In this study, we unveiled a previously unrecognized role of *Sirt5* and its mediated succinylation of CPT2 in the context of cardiac lipotoxicity and DbCM. We observed an upregulation of *Sirt5* in the myocardium of diabetic patients and mice. *Sirt5* deficiency impaired FAO, thereby contributing to myocardial lipid deposition and cardiac dysfunction in DbCM. Furthermore, a comprehensive analysis combining widely targeted metabolomics with 4D label-free proteomics and succinylomics identified CPT2 as the functional Ksuc substrate mediator of *Sirt5*, which disrupted the reconversion from fatty acyl-carnitines to fatty acyl-CoA, resulting in the accumulation of fatty acyl-carnitines and impairment of FAO. The K424R mutant inhibited *Sirt5* deficiency-mediated CPT2 succinylation and inactivation, thereby rescuing cardiac FAO and mitigating lipotoxicity. De-succinylation of CPT2 by cardiac *Sirt5* overexpression increased cardiac FAO and restored mitochondrial integrity, thereby alleviating cardiac lipotoxicity and dysfunction in DbCM.

As a severe complication of diabetes mellitus, DbCM could be evident even in patients with type 2 diabetes mellitus despite with intensive glucose control [6,7]. In DbCM, the excessive accumulation of FA and their intermediate metabolites in cardiomyocytes results in structural and functional damage to the heart [14]. Therefore, strategies aimed at mitigating the accumulation of excessive FA metabolites in cardiomyocytes prevent the development of DbCM and could potentially serve as an adjunctive treatment. However, the mechanisms governing lipid accumulation during the development of DbCM remain elusive. In this study, we have unveiled a novel role of *Sirt5*/CPT2 in mitigating cardiac lipotoxicity and DbCM for the first time, which represents the most significant finding of our research. Importantly, the observed upregulation of myocardial *Sirt5* in db/db mice could potentially have compensatory significance, akin to other established mechanisms (e.g., elevation of brain natriuretic peptide in HF). The failure to correct DbCM despite the increase in *Sirt5* levels could be attributed to the modest degree of upregulation (<1.5-fold compared to control). This view point is supported by a recent study reporting the beneficial effect of *Sirt5* in improving glucose metabolism in DbCM [36]. Based on our findings, *Sirt5* could represent a promising target for the treatment of DbCM and may have potential applications in other diseases related to ectopic fat deposition. However, it is worthy to notice that the compensatory effects of *Sirt5* are inferred from the db/db mice, and it should be interpreted with caution in other DbCM model.

Cardiomyocytes are weak in synthesizing or storing FA independently, and the uptake and metabolism of FA are tightly regulated and dynamically balanced [14,37]. FAO is the main pathway for cardiomyocytes to metabolize FA. Therefore, the immediate utilization of FA uptake for FAO is crucial, and any disruption in this process can lead to metabolic inflexibility in cardiomyocytes [14,37]. Impaired FAO can result in the incomplete oxidation of fatty acids, leading to the production of toxic intermediate metabolites and the formation of lipid droplets in cardiomyocytes [14,37]. Therefore, it seems to be reasonable to speculate that increased FAO could protect the heart from dysfunction in the context of DbCM. However, the roles of FAO in the development of DbCM have been under sharply debating. Increased cardiac FAO has long been implicated as the culprit in the generation of reactive oxygen species, resulting in oxidative damage and mitochondrial dysfunction [38]. However, this notion has been challenged by a number of studies during recent years. For one hand, decrease of FAO do not necessary benefit cardiac function. It has been reported that decrease of FAO, either by depletion of CPT1 to directly reduce FAO, or by over-expression of glucose transporter 1 to increase glucose metabolism that reduce FAO in an indirect manner, exacerbate cardiac lipotoxicity and cardiac dysfunctio [39,40]. In line with these evidences, there are studies showing that increasing cardiac FAO do not lead to mitochondrial or cardiac dysfunction either in non-obese mice [39] or HFD-induced mice [41]. For the other hand, Shao et al. showed that increasing FAO through cardiac-specific acetyl coenzyme A carboxylase 2 deletion prevented HFD-induced cardiomyopathy by preserving mitochondrial function [42]. The underlying reasons for these conflict results were unknown and animal model could not be the point since most of them are using the similar models [17,38–40] and the targets for regulating FAO are the main difference among them. Therefore, the targets for FAO regulation may be crucial in determining FAO changes and cardiac results.

All of these studies underscore the pivotal role of targeting FAO to alleviate DbCM and our study propose a novel clue. We identified that CPT2 is a novel functional substrate mediator of *Sirt5* in the regulation of FAO. CPT2, which facilitates the translocation of FA intermediate metabolites into mitochondrial matrix [43], is critical for FAO. A systematically pharmacological inhibition of CPT2 exacerbated cardiac

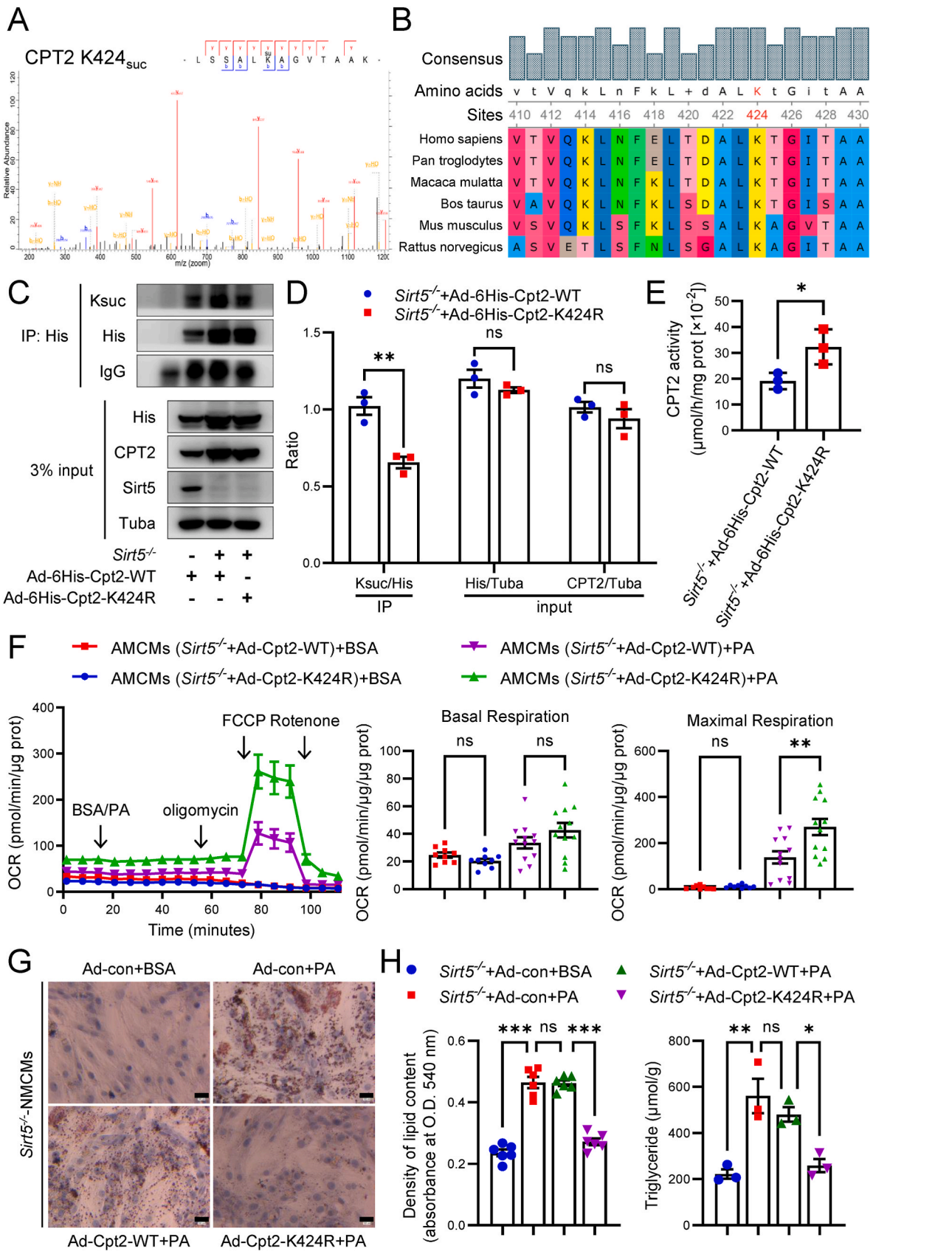

(caption on next page)

Fig. 8. The role of CPT2 Lys424 Ksuc in *Sirt5* regulating cardiac FAO and lipotoxicity. A, Mass spectrum of succinylated Lys424 of CPT2 in the succinylomics. **B**, Homology analysis of Lys424 of CPT2 across different species. **C**, Representative IP and Western blot of Ksuc and proteins expression levels of myocardial exogenous His-tagged CPT2 in WT and *Sirt5*$^{-/-}$ mice that were transfected with adenovirus expressing His-tagged WT CPT2 or K424R CPT2 (n = 3/groups). TUBA was used as the loading control. Rabbit IgG was used as the IP control. **D**, Statistical analysis of the IP and Western blot. **E**, Statistical analysis of myocardial CPT2 activity in *Sirt5*$^{-/-}$ mice that were transfected with adenovirus expressing His-tagged WT or K424R CPT2 (n = 3/groups). **F**, Seahorse metabolic analysis of FAO of AMCMs, that were isolated from *Sirt5*$^{-/-}$ mice transfected with adenovirus expressing WT or K424R CPT2 (n = 3/groups, 3–4 wells/mouse), at the presence of BSA or PA. **G**, Representative images of Oil red O staining in *Sirt5*$^{-/-}$ NMCMs that were transfected with control adenovirus or adenovirus expressing WT or K424R CPT2, at the presence of BSA or PA. Scale bar: 100 μm. **H**, Statistical analysis of optical density at 540 nm of stained Oil red O dye that was extracted by absolute isopropanol of the above NMCMs (n = 6/group) (*left*). Statistical analysis of TG concentration in the above NMCMs (n = 3/group) (*right*). Data are expressed as mean ± SEM. ns, not significant, $^{*}P < 0.05$, $^{**}P < 0.01$, $^{***}P < 0.001$. Data in **D** and **E** were analyzed using Student's t-test. Data in **F** and **H** was analyzed using one-way ANOVA followed by Bonferroni post hoc analysis. (For interpretation of the references to color in this figure legend, the reader is referred to the Web version of this article.)

dysfunction in endotoxaemia [44] but its role in DbCM has not been reported previously. Among most of the critical proteins involved in FAO, we demonstrated that CPT2 is the only substrate for *Sirt5*. Firstly, it is reasonable to exclude CPT1a and CTP1b as functional substrate proteins of *Sirt5*, as no succinylated site or a site with low intensity was detected in the succinylomics. Furthermore, other FAO key enzymes, namely acyl-CoA synthetase, acyl-CoA dehydrogenase, enoyl-CoA hydratase, 3-hydroxyacyl-CoA dehydrogenase, and 3-aceyl-CoA acetyltransferase were also excluded, as no significant change in fatty acyl-CoA levels could be observed in the metabolomics, despite being succinylated at multiple lysine sites following *Sirt5* deficiency in the succinylomics. Therefore, with robust evidence presented in the current study, we identified that CPT2 was the most important downstream substrate for *Sirt5*-dependent FAO enhancement. Besides, we provided evidence, for the first time, that succinylation regulation of CPT2 was critical for its function and FAO. Despite the presence of lysine residues (Lys424) that could be susceptible to succinylation by *Sirt5*, there is currently no experimental evidence supporting this hypothesis in previous studies. In line with our findings that the succinylation of Lys424 inactivated the enzyme activity of CPT2 and impaired cardiac FAO, it is previously reported that the lysine 79 acetylation of CPT2 leads to the accumulation of fatty acyl-carnitines [45], indicating that the PTM of a single amino acid is sufficient to disrupt CPT2 activity. Therefore, CPT2 represents a novel functional succinyl substrate mediator of *Sirt5* in the regulation of cardiac FAO in the context of DbCM.

In conclusion, we have demonstrated a novel role of *Sirt5* in preventing DbCM and uncovered a novel functional Ksuc substrate mediator CPT2 of *Sirt5* in regulating FAO. *Sirt5* deficiency impairs FAO by succinylating CPT2 at Lys424, which exacerbates cardiac lipotoxicity and DbCM. These findings highlight *Sirt5* and CPT2 as promising novel targets for the treatment of DbCM.

FUNDING

This work was supported by the National Natural Science Foundation of China to Maoxiong Wu (Grant No. 82100369), Yangxin Chen (Grant No. U23A20397, 81970200 and 82271609), Jingfeng Wang (Grant No. 82070237 and 82270254), Haifeng Zhang (Grant No. 82371573), and Jing Tan (Grant No. 82200289); the Guangdong Basic and Applied Basic Research Foundation to Maoxiong Wu (Grant No. 2019A1515110129, 2023A1515010310, and 2024A1515030240), Jing Tan (Grant No. 2021A1515110233), Haifeng Zhang (Grant No. 2020A1515011237) and Zhiteng Chen (Grant No. 2021A1515111092); the Guangzhou Science and Technology Projects to Maoxiong Wu (Grant No. 2024A04J4767); the Guangzhou Science and Technology Plan Project to Yangxin Chen (Grant No. 2023B01J1011); the Guangzhou Key Laboratory of Molecular Mechanism and Translation in Major Cardiovascular Disease to Jingfeng Wang (Grant No. 202102010007); the Guangzhou Regenerative Medicine and Health Guangdong Laboratory to Jingfeng Wang (Grant No. 2019GZR110406004), the Fundamental Research Funds for the Central Universities, Sun Yat-sen University to Maoxiong Wu (Grant No. 23qnpy140).

CRediT authorship contribution statement

Maoxiong Wu: Writing – review & editing, Writing – original draft, Project administration, Methodology, Investigation, Funding acquisition, Conceptualization. **Jing Tan:** Methodology, Investigation, Funding acquisition. **Zhengyu Cao:** Methodology, Investigation. **Yangwei Cai:** Methodology, Investigation. **Zhaoqi Huang:** Methodology, Investigation. **Zhiteng Chen:** Methodology, Investigation. **Wanbing He:** Methodology, Investigation. **Xiao Liu:** Methodology, Investigation. **Yuan Jiang:** Methodology, Investigation. **Qingyuan Gao:** Methodology, Investigation. **Bingqing Deng:** Methodology, Investigation. **Jingfeng Wang:** Writing – review & editing, Supervision, Project administration, Funding acquisition, Conceptualization. **Woliang Yuan:** Writing – review & editing, Supervision, Funding acquisition. **Haifeng Zhang:** Writing – review & editing, Supervision, Project administration, Funding acquisition, Conceptualization. **Yangxin Chen:** Writing – review & editing, Supervision, Project administration, Funding acquisition, Conceptualization.

Declaration of competing interest

The authors declare that they have no conflict of interest.

Data availability

Data will be made available on request.

Acknowledgements

None.

Appendix A. Supplementary data

Supplementary data to this article can be found online at https://doi.org/10.1016/j.redox.2024.103184.

References

[1] C.C. Low Wang, C.N. Hess, W.R. Hiatt, A.B. Goldfine, Clinical update: cardiovascular disease in diabetes mellitus: atherosclerotic cardiovascular disease and heart failure in type 2 diabetes mellitus - mechanisms, management, and clinical considerations, Circulation 133 (24) (2016) 2459–2502.

[2] R. Zou, J. Tao, J. He, C. Wang, S. Tan, Y. Xia, X. Chang, R. Li, G. Wang, H. Zhou, X. Fan, PGAM5-Mediated PHB2 dephosphorylation contributes to diabetic cardiomyopathy by disrupting mitochondrial quality surveillance, Research (2022), https://doi.org/10.34133/research.0001, 2022:Article 0001.

[3] M.M.Y. Lee, J.J.V. McMurray, A. Lorenzo-Almoros, S.L. Kristensen, N. Sattar, P. S. Jhund, M.C. Petrie, Diabetic cardiomyopathy, Heart 105 (4) (2019) 337–345.

[4] Y. Tan, Z. Zhang, C. Zheng, K.A. Wintergerst, B.B. Keller, L. Cai, Mechanisms of diabetic cardiomyopathy and potential therapeutic strategies: preclinical and clinical evidence, Nat. Rev. Cardiol. 17 (9) (2020) 585–607.

[5] H.C. Kenny, E.D. Abel, Heart failure in type 2 diabetes mellitus, Circ. Res. 124 (1) (2019) 121–141.

[6] G. Control, F.M. Turnbull, C. Abraira, R.J. Anderson, R.P. Byington, J.P. Chalmers, W.C. Duckworth, G.W. Evans, H.C. Gerstein, R.R. Holman, T.E. Moritz, B.C. Neal, T. Ninomiya, A.A. Patel, S.K. Paul, F. Travert, M. Woodward, Intensive glucose control and macrovascular outcomes in type 2 diabetes, Diabetologia 52 (11) (2009) 2288–2298.

[7] R.E. Gilbert, H. Krum, Heart failure in diabetes: effects of anti-hyperglycaemic drug therapy, Lancet 385 (9982) (2015) 2107–2117.
[8] G. Jia, M.A. Hill, J.R. Sowers, Diabetic cardiomyopathy: an update of mechanisms contributing to this clinical entity, Circ. Res. 122 (4) (2018) 624–638.
[9] R. Marfella, C. Amarelli, F. Cacciatore, M.L. Balestrieri, G. Mansueto, N. D'Onofrio, S. Esposito, I. Mattucci, G. Salerno, M. De Feo, M. D'Amico, P. Golino, C. Maiello, G. Paolisso, C. Napoli, Lipid accumulation in hearts transplanted from nondiabetic donors to diabetic recipients, J. Am. Coll. Cardiol. 75 (11) (2020) 1249–1262.
[10] A. Fukushima, G.D. Lopaschuk, Cardiac fatty acid oxidation in heart failure associated with obesity and diabetes, Biochim. Biophys. Acta 1861 (10) (2016) 1525–1534.
[11] A.C. Carpentier, Abnormal myocardial dietary fatty acid metabolism and diabetic cardiomyopathy, Can. J. Cardiol. 34 (5) (2018) 605–614.
[12] Q.G. Karwi, Q. Sun, G.D. Lopaschuk, The contribution of cardiac fatty acid oxidation to diabetic cardiomyopathy severity, Cells 10 (11) (2021).
[13] T. Wu, Y. Qu, S. Xu, Y. Wang, X. Liu, D. Ma, SIRT6: a potential therapeutic target for diabetic cardiomyopathy, Faseb. J. 37 (8) (2023) e23099.
[14] R.H. Ritchie, E.D. Abel, Basic mechanisms of diabetic heart disease, Circ. Res. 126 (11) (2020) 1501–1525.
[15] G.D. Lopaschuk, Q.G. Karwi, R. Tian, A.R. Wende, E.D. Abel, Cardiac energy metabolism in heart failure, Circ. Res. 128 (10) (2021) 1487–1513.
[16] V. Lionetti, A. Linke, M.P. Chandler, M.E. Young, M.S. Penn, S. Gupte, C. d'Agostino, T.H. Hintze, W.C. Stanley, F.A. Recchia, Carnitine palmitoyl transferase-I inhibition prevents ventricular remodeling and delays decompensation in pacing-induced heart failure, Cardiovasc. Res. 66 (3) (2005) 454–461.
[17] M. Schwarzer, G. Faerber, T. Rueckauer, D. Blum, G. Pytel, F.W. Mohr, T. Doenst, The metabolic modulators, Etomoxir and NVP-LAB121, fail to reverse pressure overload induced heart failure in vivo, Basic Res. Cardiol. 104 (5) (2009) 547–557.
[18] M. Turcani, H. Rupp, Modification of left ventricular hypertrophy by chronic etomixir treatment, Br. J. Pharmacol. 126 (2) (1999) 501–507.
[19] P.E. Wolkowicz, F. Urthaler, C. Forrest, H. Shen, J. Durand, C.C. Wei, S. Oparil, L. J. Dell'Italia, 2-Tetradecylglycidic acid, an inhibitor of carnitine palmitoyltransferase-1, induces myocardial hypertrophy via the AT1 receptor, J. Mol. Cell. Cardiol. 31 (8) (1999) 1405–1412.
[20] A.E. Kane, D.A. Sinclair, Sirtuins and NAD(+) in the development and treatment of metabolic and cardiovascular diseases, Circ. Res. 123 (7) (2018) 868–885.
[21] H. Karbasforooshan, G. Karimi, The role of SIRT1 in diabetic cardiomyopathy, Biomed. Pharmacother. 90 (2017) 386–392.
[22] Q. Yuan, L. Zhan, Q.Y. Zhou, L.L. Zhang, X.M. Chen, X.M. Hu, X.C. Yuan, SIRT2 regulates microtubule stabilization in diabetic cardiomyopathy, Eur. J. Pharmacol. 764 (2015) 554–561.
[23] A. Kanwal, V.B. Pillai, S. Samant, M. Gupta, M.P. Gupta, The nuclear and mitochondrial sirtuins, Sirt6 and Sirt3, regulate each other's activity and protect the heart from developing obesity-mediated diabetic cardiomyopathy, Faseb. J. 33 (10) (2019) 10872–10888.
[24] N. Nasrin, X. Wu, E. Fortier, Y. Feng, O.C. Bare, S. Chen, X. Ren, Z. Wu, R. S. Streeper, L. Bordone, SIRT4 regulates fatty acid oxidation and mitochondrial gene expression in liver and muscle cells, J. Biol. Chem. 285 (42) (2010) 31995–32002.
[25] S. Sadhukhan, X. Liu, D. Ryu, O.D. Nelson, J.A. Stupinski, Z. Li, W. Chen, S. Zhang, R.S. Weiss, J.W. Locasale, J. Auwerx, H. Lin, Metabolomics-assisted proteomics identifies succinylation and SIRT5 as important regulators of cardiac function, Proc. Natl. Acad. Sci. U. S. A. 113 (16) (2016) 4320–4325.
[26] T. Yoshizawa, M.F. Karim, Y. Sato, T. Senokuchi, K. Miyata, T. Fukuda, C. Go, M. Tasaki, K. Uchimura, T. Kadomatsu, Z. Tian, C. Smolka, T. Sawa, M. Takeya, K. Tomizawa, Y. Ando, E. Araki, T. Akaike, T. Braun, Y. Oike, E. Bober, K. Yamagata, SIRT7 controls hepatic lipid metabolism by regulating the ubiquitin-proteasome pathway, Cell Metabol. 19 (4) (2014) 712–721.
[27] K.A. Hershberger, D.M. Abraham, A.S. Martin, L. Mao, J. Liu, H. Gu, J.W. Locasale, M.D. Hirschey, Sirtuin 5 is required for mouse survival in response to cardiac pressure overload, J. Biol. Chem. 292 (48) (2017) 19767–19781.
[28] M.X. Wu, S.H. Wang, Y. Xie, Z.T. Chen, Q. Guo, W.L. Yuan, C. Guan, C.Z. Xu, Y. N. Huang, J.F. Wang, H.F. Zhang, Y.X. Chen, Interleukin-33 alleviates diabetic cardiomyopathy through regulation of endoplasmic reticulum stress and autophagy via insulin-like growth factor-binding protein 3, J. Cell. Physiol. 236 (6) (2021) 4403–4419.
[29] H.Y. Fu, S. Sanada, T. Matsuzaki, Y. Liao, K. Okuda, M. Yamato, S. Tsuchida, R. Araki, Y. Asano, H. Asanuma, M. Asakura, B.A. French, Y. Sakata, M. Kitakaze, T. Minamino, Chemical endoplasmic reticulum chaperone alleviates doxorubicin-induced cardiac dysfunction, Circ. Res. 118 (5) (2016) 798–809.
[30] S.H. Wang, X.L. Zhu, F. Wang, S.X. Chen, Z.T. Chen, Q. Qiu, W.H. Liu, M.X. Wu, B. Q. Deng, Y. Xie, J.T. Mai, Y. Yang, J.F. Wang, H.F. Zhang, Y.X. Chen, LncRNA H19 governs mitophagy and restores mitochondrial respiration in the heart through Pink1/Parkin signaling during obesity, Cell Death Dis. 12 (6) (2021) 557.
[31] L. Jin, L. Geng, L. Ying, L. Shu, K. Ye, R. Yang, Y. Liu, Y. Wang, Y. Cai, X. Jiang, Q. Wang, X. Yan, B. Liao, J. Liu, F. Duan, G. Sweeney, C.W.H. Woo, Y. Wang, Z. Xia, Q. Lian, A. Xu, FGF21-Sirtuin 3 Axis confers the protective effects of exercise against diabetic cardiomyopathy by governing mitochondrial integrity, Circulation 146 (20) (2022) 1537–1557.
[32] X. Li, Y. Wu, J. Zhao, H. Wang, J. Tan, M. Yang, Y. Li, S. Deng, S. Gao, H. Li, Z. Yang, F. Yang, J. Ma, J. Cheng, W. Cai, Distinct cardiac energy metabolism and oxidative stress adaptations between obese and non-obese type 2 diabetes mellitus, Theranostics 10 (6) (2020) 2675–2695.
[33] L.H. Yang, R.J. Dong, Y.W. Lu, H.M. Wang, Y.Q. Kuang, R.R. Wang, Y.Y. Li, Integration of metabolomics and transcriptomics analyses reveals sphingosine-1-phosphate-mediated S1PR2/PI3K/Akt pathway involved in Talaromyces marneffei infection of macrophages, Microb. Pathog. 175 (2023) 105985.
[34] Y. Song, L. Sun, H. Wang, S. Zhang, K. Fan, Y. Mao, J. Zhang, X. Han, H. Chen, Y. Xu, K. Sun, Z. Ding, Y. Wang, Enzymatic fermentation of rapeseed cake significantly improved the soil environment of tea rhizosphere, BMC Microbiol. 23 (1) (2023) 250.
[35] J. Suzuki, Effects of hyperbaric environment on endurance and metabolism are exposure time-dependent in well-trained mice, Phys. Rep. 9 (5) (2021) e14780.
[36] C. Wei, M. Shi, S. Dong, Z. Li, B. Zhao, D. Liu, G. Li, J. Cen, L. Yu, X. Liang, L. Shi, SIRT5-related lysine demalonylation of GSTP1 contributes to cardiomyocyte pyroptosis suppression in diabetic cardiomyopathy, Int. J. Biol. Sci. 20 (2) (2024) 585–605.
[37] P.M. Seferovic, W.J. Paulus, Clinical diabetic cardiomyopathy: a two-faced disease with restrictive and dilated phenotypes, Eur. Heart J. 36 (27) (2015) 1718–1727, 1727a-1727.
[38] P.K. Mazumder, B.T. O'Neill, M.W. Roberts, J. Buchanan, U.J. Yun, R.C. Cooksey, S. Boudina, E.D. Abel, Impaired cardiac efficiency and increased fatty acid oxidation in insulin-resistant ob/ob mouse hearts, Diabetes 53 (9) (2004) 2366–2374.
[39] S.C. Kolwicz Jr., D.P. Olson, L.C. Marney, L. Garcia-Menendez, R.E. Synovec, R. Tian, Cardiac-specific deletion of acetyl CoA carboxylase 2 prevents metabolic remodeling during pressure-overload hypertrophy, Circ. Res. 111 (6) (2012) 728–738.
[40] J. Yan, M.E. Young, L. Cui, G.D. Lopaschuk, R. Liao, R. Tian, Increased glucose uptake and oxidation in mouse hearts prevent high fatty acid oxidation but cause cardiac dysfunction in diet-induced obesity, Circulation 119 (21) (2009) 2818–2828.
[41] Z. Liu, J. Ding, T.S. McMillen, O. Villet, R. Tian, D. Shao, Enhancing fatty acid oxidation negatively regulates PPARs signaling in the heart, J. Mol. Cell. Cardiol. 146 (2020) 1–11.
[42] D. Shao, S.C. Kolwicz Jr., P. Wang, N.D. Roe, O. Villet, K. Nishi, Y.A. Hsu, G. V. Flint, A. Caudal, W. Wang, M. Regnier, R. Tian, Increasing fatty acid oxidation prevents high-fat diet-induced cardiomyopathy through regulating parkin-mediated mitophagy, Circulation 142 (10) (2020) 983–997.
[43] I. Zlobine, K. Gopal, J.R. Ussher, Lipotoxicity in obesity and diabetes-related cardiac dysfunction, Biochim. Biophys. Acta 1861 (10) (2016) 1555–1568.
[44] M. Makrecka-Kuka, S. Korzh, M. Videja, R. Vilskersts, E. Sevostjanovs, O. Zharkova-Malkova, P. Arsenyan, J. Kuka, M. Dambrova, E. Liepinsh, Inhibition of CPT2 exacerbates cardiac dysfunction and inflammation in experimental endotoxaemia, J. Cell Mol. Med. 24 (20) (2020) 11903–11911.
[45] X. Fan, Y. Wang, X. Cai, Y. Shen, T. Xu, Y. Xu, J. Cheng, X. Wang, L. Zhang, J. Dai, S. Lin, J. Liu, CPT2 K79 acetylation regulates platelet life span, Blood Adv 6 (17) (2022) 4924–4935.